

# 1 **Impact of reactive surfaces on the abiotic reaction between nitrite and** 2 **ferrous iron and associated nitrogen and oxygen isotope dynamics**

3 Anna-Neva Visser<sup>1,4</sup>, Scott D. Wankel<sup>2</sup>, Pascal A. Niklaus<sup>3</sup>, James M. Byrne<sup>4</sup>, Andreas A. Kappler<sup>4</sup>,  
4 Moritz F. Lehmann<sup>1</sup>

5 <sup>1</sup>Department of Environmental Sciences, Basel University, Bernoullistrasse 30, 4056 Basel, Switzerland

6 <sup>2</sup>Woods Hole Oceanographic Institution, Woods Hole, 360 Woods Hole Rd, MA 02543, USA

7 <sup>3</sup>Department of Evolutionary Biology and Environmental Studies, University of Zürich, Winterthurerstrasse 190, 8057 Zürich,  
8 Switzerland

9 <sup>4</sup>Department of Geosciences, Tübingen University, Hölderlinstrasse 12, 72074 Tübingen, Germany

10 *Correspondence to:* Anna-Neva Visser (a.visser@unibas.ch)

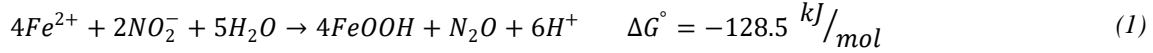
11 **Abstract.** Anaerobic nitrate-dependent Fe(II) oxidation (NDFeO) is widespread in various aquatic environments, and plays a  
12 major role in iron and nitrogen redox dynamics. However, evidence for truly enzymatic, autotrophic NDFeO remains limited,  
13 with alternative explanations involving coupling of heterotrophic denitrification with abiotic oxidation of structurally-bound  
14 or aqueous Fe(II) by reactive intermediate N species (chemodenitrification). The extent to which chemodenitrification is  
15 caused, or enhanced, by *ex vivo* surface catalytic effects has, so far, not been directly tested. To determine whether the presence  
16 of either a Fe(II)-bearing mineral or dead biomass (DB) catalyses chemodenitrification, two different sets of anoxic batch  
17 experiments were conducted: 2 mM Fe(II) was added to a low-phosphate medium, resulting in the precipitation of vivianite  
18 ( $\text{Fe}_3(\text{PO}_4)_2$ ), to which later 2 mM nitrite ( $\text{NO}_2^-$ ) was added, with or without an autoclaved cell suspension ( $\sim 1.96 \times 10^8$  cells  $\text{ml}^{-1}$   
19 <sup>1</sup>) of *Shewanella oneidensis* MR-1. Concentrations of nitrite, nitrous oxide ( $\text{N}_2\text{O}$ ) and iron ( $\text{Fe}^{2+}$ ,  $\text{Fe}_{\text{tot}}$ ) were monitored over  
20 time in both setups to assess the impact of Fe(II) minerals and/or DB as catalysts of chemodenitrification. In addition, the  
21 natural-abundance isotope ratios of  $\text{NO}_2^-$  and  $\text{N}_2\text{O}$  ( $\delta^{15}\text{N}$  and  $\delta^{18}\text{O}$ ) were analysed to constrain associated isotope effects. Up  
22 to 90% of the Fe(II) was oxidized in the presence of DB, while only ~65% were oxidized under mineral-only conditions,  
23 suggesting an overall lower reactivity of the mineral-only setup. Similarly, the average  $\text{NO}_2^-$  reduction rate in the mineral-only  
24 experiments ( $0.004 \pm 0.003$  mmol  $\text{L}^{-1}$  day<sup>-1</sup>) was much lower compared to experiments with mineral plus DB ( $0.053 \pm 0.013$   
25 mmol  $\text{L}^{-1}$  day<sup>-1</sup>), as was  $\text{N}_2\text{O}$  production ( $204.02 \pm 60.29$  nmol/L\*day). The  $\text{N}_2\text{O}$  yield per mole  $\text{NO}_2^-$  reduced was higher in  
26 the mineral-only setups (4%) compared to the experiments with DB (1%), suggesting the catalysis-dependent differential  
27 formation of NO. N- $\text{NO}_2^-$  isotope ratio measurements indicated a clear difference between both experimental conditions: In  
28 contrast to the marked <sup>15</sup>N isotope enrichment during active  $\text{NO}_2^-$  reduction ( $^{15}\epsilon_{\text{NO}_2} = +10.3\text{‰}$ ) observed in the presence of DB,  
29  $\text{NO}_2^-$  loss in the mineral-only experiments exhibited only a small N isotope effect ( $< +1\text{‰}$ ). The  $\text{NO}_2^-$ -O isotope effect was  
30 very low in both setups ( $^{18}\epsilon_{\text{NO}_2} < 1\text{‰}$ ), most likely due to substantial O isotope exchange with ambient water. Moreover, during  
31 the low-turnover conditions (i.e. in the mineral-only experiments, as well as initially in experiments with DB), the observed  
32  $\text{NO}_2^-$  isotope systematics suggest, transiently, a small inverse isotope effect (i.e. decreasing  $\text{NO}_2^-$   $\delta^{15}\text{N}$  and  $\delta^{18}\text{O}$  with decreasing

concentrations), possibly related to transitory surface complexation mechanisms. Site preference (SP) of the  $^{15}\text{N}$  isotopes in the linear  $\text{N}_2\text{O}$  molecule for both setups ranged between 0 to 14‰, notably lower than previously reported for chemodenitrification. Our results imply that chemodenitrification is dependent on the available reactive surfaces, and that the  $\text{NO}_2^-$  (rather than the  $\text{N}_2\text{O}$ ) isotope signatures may be useful for distinguishing between chemodenitrification catalysed by minerals, chemodenitrification catalysed by dead microbial biomass, and possibly true enzymatic NDFeO.

## 1. Introduction

Iron (Fe) is essential for all living beings and its biogeochemical cycling has been studied extensively (Expert, 2012; Lovley, 1997). Although Fe is ubiquitous in most environments, it is not always bioavailable (Andrews et al., 2003; Ilbert and Bonnefoy, 2013), and microorganisms must often cope with Fe limitation in their respective environments (Braun and Hantke, 2013; Ilbert and Bonnefoy, 2013). This is especially true at circumneutral pH and oxic conditions, where Fe(II) is quickly oxidized by  $\text{O}_2$  and thus only present as poorly soluble Fe(III)(oxyhydr)oxides (Cornell and Schwertmann, 2003; Stumm and Sulzberger, 1992). In contrast, under anoxic conditions, Fe is mainly present as either dissolved  $\text{Fe}^{2+}$  or as mineral-bound Fe(II) in Fe phosphates or carbonates (Charlet et al., 1990; Luna-Zaragoza et al., 2009). Here, microbes use electron acceptors other than  $\text{O}_2$  for respiration (He et al., 2016; Lovley, 2012; Straub et al., 1996). One redox pair that has been proposed to be exploited by microbes under anoxic conditions is  $\text{NO}_3^-/\text{Fe}^{2+}$ , through a mechanism known as nitrate-dependent Fe(II) oxidation (NDFeO) (Ilbert and Bonnefoy, 2013; Straub et al., 1996). To date, genetic evidence that clearly supports this metabolic capacity of the studied microorganisms remains lacking (Price et al., 2018), and biogeochemical evidence is rare and putative. The latter is mostly based on experiments with the chemolithoautotrophic culture KS, a consortium of four different strains, including a relative of the microaerophilic *Sideroxydans/Gallionella*. This enrichment culture has been shown to oxidize Fe(II) without the addition of any organic co-substrates (Tominski et al., 2018). Tian et al. (2020) confirmed that *Gallionellaceae* are able to perform autotrophic Fe(II)-dependent denitrification. Another more indirect line of evidence includes results from slurry microcosm experiments with marine coastal sediments. In these experiments, Fe(II) oxidation was still detected even after all bioavailable organics of the sediments were consumed and only  $\text{NO}_3^-$  was left (Laufer et al., 2016). With regards to other studies where NDFeO was initially thought to be performed by autotrophs (Chakraborty et al., 2011; Weber et al., 2009), it was subsequently shown that the microbes rely on an organic co-substrate and must in fact be considered mixotrophic (Klueglein et al., 2014; Muehe et al., 2009). Yet, the exact mechanism promoting NDFeO in the microorganisms that have been investigated so far (e.g. *Acidovorax delafieldii* strain 2AN, *Pseudogulbenkiania ferrooxidans* strain 2002) (Chakraborty et al., 2011; Weber et al., 2009), is still not fully understood. It has been suggested that extracellular electron transfer (EET) might play a major role in NDFeO, particularly in the presence of high levels of extracellular polymeric substances (EPS) (Klueglein et al., 2014; Liu et al., 2018; Zeitvogel et al., 2017). EPS have been demonstrated to act as electron shuttles, hence EET may indeed provide a plausible explanation for the observed Fe(II) oxidation in these cultures (Liu et al., 2018). The existence of such an electron transfer would imply that NDFeO is not necessarily a completely enzymatically-catalysed

65 reaction. Considering that all putative NDFeO strains were grown under high (up to 10 mM) nitrate ( $\text{NO}_3^-$ ) and Fe(II)  
 66 concentrations, and accumulated up to several mM nitrite ( $\text{NO}_2^-$ ) from enzymatic  $\text{NO}_3^-$  reduction, other studies suggested that  
 67 the observed Fe(II) oxidation in these pure cultures may be due to the abiotic side reaction between the generated  $\text{NO}_2^-$  and  
 68 Fe(II) (Buchwald et al., 2016; Prakash Dhakal, 2013; Klueglein et al., 2014). This abiotic reaction between  $\text{NO}_2^-$  and Fe(II) is  
 69 known as chemodenitrification (Equation 1) and is proposed to lead to an enhanced production of  $\text{N}_2\text{O}$  (Anderson and Levine,  
 70 1986; Buchwald et al., 2016; Zhu-Barker et al., 2015).



71 Several studies have noted that the presence of reactive surfaces may enhance the abiotic reaction (Heil et al., 2016; Sorensen  
 72 and Thorling, 1991). For example, Klueglein and Kappler (2013) tested the impact of goethite on Fe-coupled  
 73 chemodenitrification in the presence of high Fe(II) and  $\text{NO}_2^-$  concentrations, and confirmed the concentration dependency of  
 74 this reaction with regard to both species (Van Cleemput and Samater, 1995). Possible catalytic effects (e.g. by reactive surfaces  
 75 and/or organic matter) were not tested specifically in these studies. Yet, multiple factors have been shown to affect the abiotic  
 76 reaction between  $\text{NO}_2^-$  and Fe(II) and may need to be considered (i.e. pH, temperature,  $\text{Fe}^{2+}$  concentrations, solubility of  
 77 Fe(III)(oxyhydr)oxides, crystallinity of Fe(II) minerals, other metal ion concentrations and catalytic effects) (Van Cleemput  
 78 & Samater, 1995; Klueglein & Kappler, 2013; Ottley et al., 1997). In addition, the presence of organic compounds can lead to  
 79 the abiotic reduction of  $\text{NO}_2^-$  to NO (Van Cleemput and Samater, 1995; McKnight et al., 1997; Pereira et al., 2013).

80 Given the complex controls and potential interaction between Fe(II) and various nitrogenous compounds, including  
 81 intermediates, it may be an oversimplification to state that Fe(II) oxidation observed in previous laboratory setups is solely  
 82 caused by the abiotic reaction with  $\text{NO}_2^-$ , and not, for example, stimulated by reactive surfaces (minerals, organic-detritus) or  
 83 by nitric oxide (NO), a highly reactive intermediate not easily quantified in anoxic batch experiments. In order to better  
 84 understand the factors that may control chemodenitrification of  $\text{NO}_2^-$ , this study focuses on the possible catalytic surface effects  
 85 induced by a Fe(II) mineral phase or dead biomass (DB). Furthermore, microbial cells, DB, or detrital waste products might  
 86 not only provide additional reactive surface area, but may directly react with  $\text{NO}_2^-$  to form NO.

87 Stable isotopes of both N and O ( $\delta^{15}\text{N}$  and  $\delta^{18}\text{O}$ ) offer a promising approach to further elucidate the mechanism of NDFeO,  
 88 and also to more generally expand our understanding of chemodenitrification. The N and O isotopic composition of  
 89 nitrogenous compounds (e.g.  $\text{NO}_3^-$ ,  $\text{NO}_2^-$ , and  $\text{N}_2\text{O}$ ) has been used to gain deeper insights into various N turnover processes  
 90 (Granger et al., 2008; Jones et al., 2015). The dual  $\text{NO}_2^-$  (or  $\text{NO}_3^-$ ) isotope approach is based on the fact that specific N-  
 91 transformation processes – biotic or abiotic – are associated with specific N and O isotope fractionation (i.e. isotope effect). In  
 92 general, enzymatic processes promote the more rapid reaction of lighter N and O isotopologues, leaving the remaining substrate  
 93 pool enriched in the heavier isotopes (i.e.  $^{15}\text{N}$ ,  $^{18}\text{O}$ ) (Granger et al., 2008; Kendall & Aravena, 2000; Martin & Casciotti, 2017).  
 94 Only a few studies exist that have looked into the isotope effects of chemodenitrification and reports on the associated isotope  
 95 effects are variable. Consistent with what we know from biological denitrification, chemodenitrification experiments with 10  
 96 mM Fe(II) and  $\text{NO}_2^-$ , and very high reaction rates, revealed a significant increase in the  $\delta^{15}\text{N}$  (up to 40‰) and  $\delta^{18}\text{O}$  (up to

30‰)  $\text{NO}_2^-$  values, corresponding to an overall N and O isotope effect of  $^{15}\epsilon$   $18.1 \pm 1.7\text{‰}$  and  $^{18}\epsilon$   $9.8 \pm 1.8\text{‰}$ , as well as a  $\Delta^{15}\text{N}$  (i.e. the difference between  $\delta^{15}\text{NO}_2^-$  and  $\delta^{15}\text{N}_2\text{O}$ ) of  $27 \pm 4.5\text{‰}$  (Jones et al., 2015). However, reaction kinetics can significantly affect isotope reaction dynamics, and chemodenitrification is possibly impacted by e.g. concentration effects and/or the presence of different catalysts (i.e. surfaces, organics). Hence, performing coupled N and O isotope measurements might help to gain deeper insights into the mechanistic details and fractionation systematics of  $\text{NO}_2^-$  reduction in the presence of Fe(II). Here, in order to expand the limited dataset on the isotope effects of abiotic Fe(II)-coupled denitrification, and in turn to lay the groundwork for using  $\text{NO}_3^-/\text{NO}_2^-$  N and O isotope measurements to unravel the mechanism behind NDFeO, we studied the N and O isotope dynamics of  $\text{NO}_2^-$  reduction and  $\text{N}_2\text{O}$  production during abiotic reaction of  $\text{NO}_2^-$  with Fe(II). As the extent of the formation of various Fe(III)(oxyhydr)oxides has been previously reported to enhance chemodenitrification dynamics (Chen et al., 2018; Sorensen and Thorling, 1991), we also followed mineral alteration during chemodenitrification in order to identify possible reaction patterns. A specific goal in this context was to assess the impact of Fe(II) precipitates and/or dead biomass as catalytic agents during Fe(II)-associated chemodenitrification, as well as potential mineral transformation processes associated with the abiotic oxidation of Fe(II) via reactive  $\text{NO}_x$  species.

## 2. Material and Methods

### 2.1. General experimental setup

For all experiments, anoxic low phosphate medium (1.03 mM  $\text{KH}_2\text{PO}_4$ , 3.42 mM NaCl, 5.61 mM  $\text{NH}_4\text{Cl}$ , 2.03 mM  $\text{MgSO}_4 \cdot 7\text{H}_2\text{O}$  and 0.68 mM  $\text{CaCl}_2 \cdot 2\text{H}_2\text{O}$ , with a 7-vitamin (Widdel & Pfennig, 1981) and a SL-10 trace element solution (Widdel et al., 1983; 22 mM bicarbonate buffered) was prepared. The medium was dispensed with a Widdel flask in 1-l Schott bottles and the pH for each bottle was adjusted separately by the addition of anoxic, sterile 1 M HCl. For both setups, five different pH values were targeted: 5.8, 6.2, 6.5, 6.9 and 7.1. After pH adjustment,  $\text{Fe(II)Cl}_2$  was added to reach a concentration of ~2 mM Fe(II), and, if necessary, the pH was re-adjusted. The medium was kept for 48 h at 4°C, resulting in amorphous, green-greyish Fe(II) precipitates. In addition, ~2 mM  $\text{NaNO}_2$  and ~1 mM Na-acetate were added to the main medium stocks shortly before 10 ml aliquots of the medium were distributed into 20 ml headspace vials (heat-sterilized) in an anoxic glove box (MBraun,  $\text{N}_2$ , 100%). Acetate was added to mimic experiments, in which bacteria are cultivated (yet, acetate concentrations did not change during incubations, underscoring that the organic acid was not involved in the observed reactions; data not shown). All headspace vials were closed with black butyl stoppers and crimp-sealed [headspace  $\text{N}_2/\text{CO}_2$  (90/10, v/v)]. All vials were then incubated at 28°C in the dark.

*Incubations with dead-biomass* – *Shewanella oneidensis* MR-1, a facultative aerobic Gram-negative bacterium, is seen as model organism for bioremediation studies due to its various respiratory abilities (Heidelberg et al., 2002; Lies et al., 2005). It is known to perform dissimilatory metal reduction by utilizing alternative terminal electron acceptors such as elemental sulfur, Mn(IV), Fe(III) or  $\text{NO}_3^-$ . Since *S. oneidensis* produces large amounts of EPS (Dai et al., 2016; Heidelberg et al., 2002), but is not capable of oxidizing Fe(II) (Lies et al., 2005; Piepenbrock et al., 2011) (i.e. no interference with abiotic reactions involving

129 Fe/chemodenitrification), we chose concentrated and sterilized *S. oneidensis* for our dead-biomass experiments. In preparation  
 130 of these experiments, *S. oneidensis* MR-1 was grown oxically on a LB (lysogeny broth) medium (10 g tryptone, 5 g yeast  
 131 extract, 10 g NaCl in 1 l DI water) in six 250 ml Erlenmeyer flasks. After 12 hrs, cultures were transferred into 50 ml Falcon  
 132 tubes and centrifuged for 25 min at  $3956.6 \times g$  (4000 rpm; Eppendorf, 5430 R, Rotor F-35-6-30). Cell-containing pellets were  
 133 washed twice with oxalic acid and centrifuged again, followed by three more washing steps with TRIS buffer prior to final  
 134 resuspension in 5 ml TRIS buffer. Pellet suspensions were pooled in a 100 ml serum bottle and autoclaved twice to ensure that  
 135 all cells were killed. Before distribution of the medium into 20 ml vials (see above), cell suspension was added to yield a cell  
 136 density of  $\sim 1.96 \times 10^8$  cell ml<sup>-1</sup>. Care was taken to ensure the homogenous distribution of mineral precipitates and the dead  
 137 biomass.

## 138 2.2. Sampling and sample preparation

139 Incubations were run for approximately 30 days, and sampling was performed in an anoxic glove box (MBraun, N<sub>2</sub>, 100%) at  
 140 five time points. For each time point, and for each pH treatment, 9 replicates were prepared. Therefore, variations between the  
 141 replicates and the different sampling time points are possible. For sampling, the headspace was quantitatively transferred into  
 142 12 ml He-purged Exetainer vials (LABCO) for N<sub>2</sub>O concentration measurements. Then, 2 ml of the liquid sample were  
 143 transferred into 2 ml Eppendorf tubes, centrifuged for 5 min ( $12100 \times g$ / 13400 rpm; Eppendorf, MiniSpin), followed by a  
 144 1:10 dilution of the supernatant in 1 ml anoxic MilliQ water for NO<sub>2</sub><sup>-</sup> quantification. A second 100 µl aliquot was diluted 1:10  
 145 in 40 mM sulfamic acid (SFA) for iron determination by ferrozine analysis (Granger and Sigman, 2009; Klueglein and Kappler,  
 146 2013). The remaining supernatant was used for HPLC and NO<sub>2</sub><sup>-</sup> isotope analysis. Finally, the spun-down pellet was  
 147 resuspended in 1 M HCl for ferrozine analysis (Stookey, 1970). All liquid samples were stored at 4°C in the dark until further  
 148 processing. The remaining liquid samples were used for <sup>57</sup>Fe Mössbauer spectroscopy.

## 149 2.3. Analytical techniques

150 *NO<sub>2</sub><sup>-</sup> concentrations* – NO<sub>2</sub><sup>-</sup> concentrations were quantified within one hour after the sample was taken via a standard  
 151 segmented continuous-flow analytical (CFA, SEAL Analytics) photometric technique (Snyder and Adler, 1976). NO<sub>2</sub><sup>-</sup>  
 152 reduction rates were calculated based on the observed net concentration decrease (  $\overline{[C]}_{t0} - \overline{[C]}_{tend} \pm \text{standard error}$ ) with time.

153 *Fe concentrations* – SFA- and/or HCl-fixed samples were stored in the dark and at 4°C until Fe(II) concentrations were  
 154 analysed using the ferrozine assay (Stookey, 1970), which was adapted for NO<sub>2</sub><sup>-</sup>-containing samples by Klueglein et al. (2013).  
 155 Total Fe(II) concentrations were calculated as the sum of the  $Fe_{aq}^{2+} + Fe(II)_{pellet}$  concentrations.

156 *N<sub>2</sub>O concentrations* – Prior to the quantification of the N<sub>2</sub>O, the sample gas was diluted (1:5) with 5.0 He. Triplicate samples  
 157 were then analysed using a gas chromatograph with an electron capture detector (GC-ECD; Agilent 7890 with micro-ECD and  
 158 FID; Porapak Q 80/100 column). GC-ECD measurements were calibrated using four standard gases containing different

159 concentrations of N<sub>2</sub>O (Niklaus et al., 2016). N<sub>2</sub>O production rates were calculated based on the observed net N<sub>2</sub>O  
160 concentration increase ( $\overline{[C]}_{tend} - \overline{[C]}_{t0} \pm \text{standard error}$ ) with time.

161 *<sup>57</sup>Fe Mössbauer spectroscopy* - For Mössbauer spectroscopic analyses, the remaining liquid samples (ca. 8 ml) were processed  
162 inside an anoxic glove box. The entire liquid including the precipitates was passed through a 0.45 µm filter. The wet filter was  
163 then sealed between two layers of Kapton tape and kept inside sealed Schott bottles in a freezer (-20°C) under anoxic conditions  
164 until analysis. From the treatments with DB, samples were collected at day 0 at pH 6.8 and at the end of the experiment (~30  
165 days) for pH 6.8 and 5.8. For the mineral-only experiment, only one sample (time point zero, pH 6.8) was analysed, as a basis  
166 for comparison with the DB experiments (i.e. to verify whether DB has an immediate effect on the mineral phase). Taking  
167 care to minimize exposure to air, samples were transferred from the air-tight Schott bottles and loaded inside a closed-cycle  
168 exchange gas cryostat (Janis cryogenics). Measurements were performed at 77 K with a constant acceleration drive system  
169 (WissEL) in transmission mode with a <sup>57</sup>Co/Rh source and calibrated against a 7µm thick α-<sup>57</sup>Fe foil measured at room  
170 temperature. All spectra were analysed using Recoil (University of Ottawa) by applying a Voight Based Fitting (VBF) routine  
171 (Lagarec and Rancourt, 1997; Rancourt and Ping, 1991). The half-width at half maximum (HWHM) was fixed to a value of  
172 0.130 mm/s during fitting.

173 *Nitrite N and O isotope measurements* – The nitrogen (N) and oxygen (O) isotope composition of NO<sub>2</sub><sup>-</sup> was determined using  
174 the azide method (McIlvin and Altabet, 2005). This method is based on the chemical conversion of NO<sub>2</sub><sup>-</sup> to gaseous N<sub>2</sub>O at a  
175 low pH (4 to 4.5) (McIlvin and Altabet, 2005), and the subsequent analysis of the concentrated and purified N<sub>2</sub>O by gas  
176 chromatography-isotope ratio mass spectrometry (GC-IRMS). Addition of 0.6 M NaCl to the acetic acid-azide solution was  
177 conducted in order to minimize oxygen isotope exchange (McIlvin and Altabet, 2005). The acetic acid-azide solution was  
178 prepared freshly every day (McIlvin and Altabet, 2005) and kept in a crimp sealed (grey butyl stopper) 50 ml serum bottle.  
179 Sample volume equivalent to 40 nmol NO<sub>2</sub><sup>-</sup> was added to pre-combusted headspace vials, filled up to 3 ml with anoxic MilliQ  
180 water, and crimp-sealed. Then, 100 µl of the acetic acid/azide solution was added. After ~7 hrs, 100 µl of 6 M NaOH was  
181 added to stop the reaction. Until isotope analysis by a modified purge and trap gas bench coupled to CF-IRMS (McIlvin and  
182 Casciotti, 2010), the samples were stored upside down at room temperature and in the dark. Two nitrite isotope standards,  
183 namely N-7373 (δ<sup>15</sup>N: -79.6‰, δ<sup>18</sup>O: +4.5‰) and N-10219 (δ<sup>15</sup>N: +2.8‰; δ<sup>18</sup>O: +88.5‰) (Casciotti & McIlvin, 2007), were  
184 prepared on the day of isotope analysis and processed the same way as samples. N and O isotope data are expressed in the  
185 common δ notation and reported as permil deviation (‰) relative to AIR N<sub>2</sub> and VSMOW, respectively ((δ<sup>15</sup>N = ([<sup>15</sup>N]/[<sup>14</sup>N])<sub>sample</sub> / [<sup>15</sup>N]/[<sup>14</sup>N]<sub>air\_N2</sub> - 1) × 1000‰ and δ<sup>18</sup>O = ([<sup>18</sup>O]/[<sup>16</sup>O])<sub>sample</sub> / [<sup>18</sup>O]/[<sup>16</sup>O]<sub>VSMOW</sub> - 1) × 1000‰). Based on replicate  
186 measurements of laboratory standards and samples, the analytical precision for NO<sub>2</sub><sup>-</sup> δ<sup>15</sup>N and δ<sup>18</sup>O analyses was ±0.4‰ and  
187 ±0.6‰ (1 SD), respectively.

189 *N<sub>2</sub>O N and O isotope measurements* – Triplicate 12 nmol samples of N<sub>2</sub>O were injected into 20 ml headspace vials that were  
190 flushed before for 5 hrs with 5.0 He (injection volumes according to the N<sub>2</sub>O concentrations determined before). The N<sub>2</sub>O was  
191 then analysed directly using CF-IRMS (see above). Two standard gases with known δ<sup>15</sup>N and δ<sup>18</sup>O values were analysed along

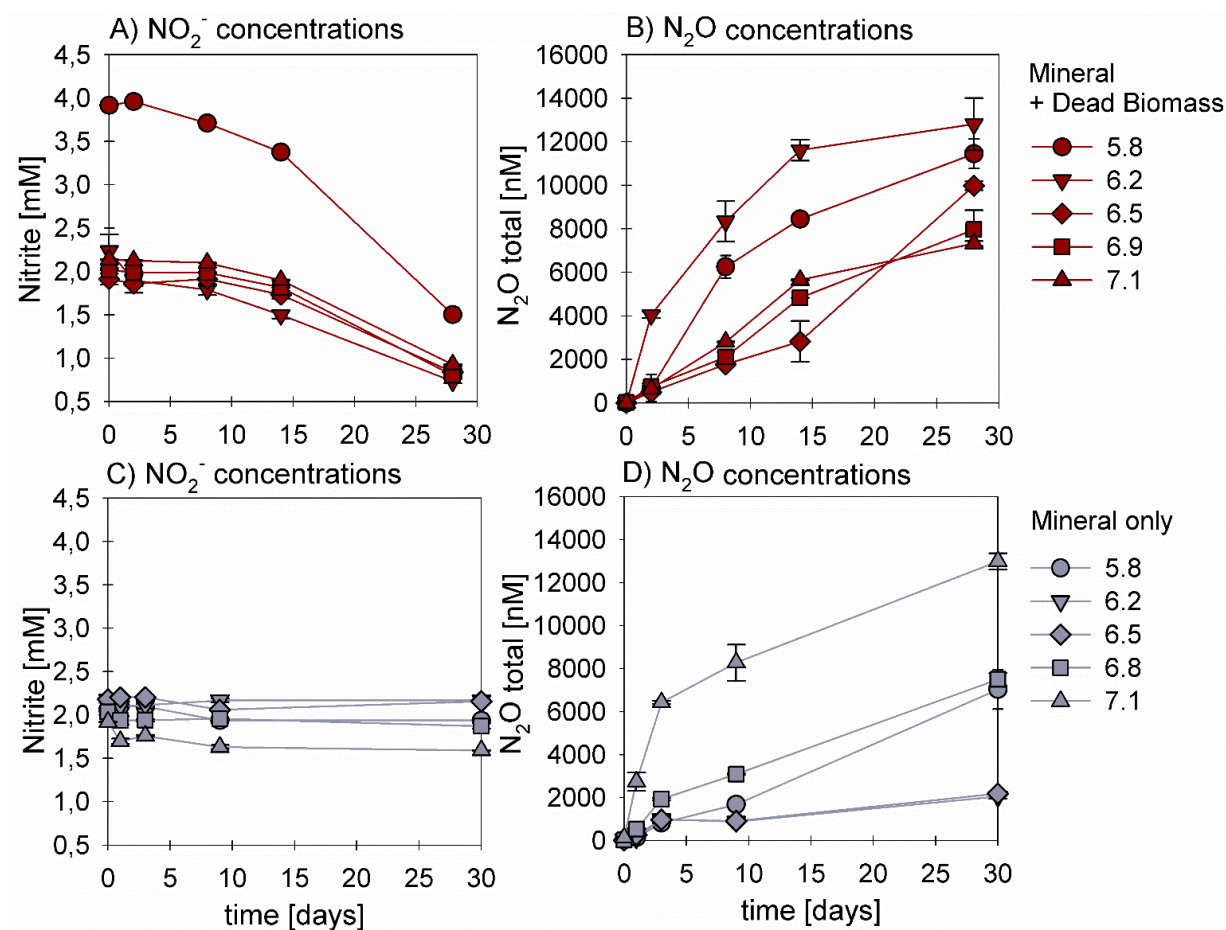
192 with the samples, namely FI.CA06261 ( $\delta^{15}\text{N}$ : -35.74‰,  $\delta^{15}\text{N}^{\alpha}$ : -22.21‰,  $\delta^{15}\text{N}^{\beta}$ =-49.28‰,  $\delta^{18}\text{O}$ : 26.94‰) and FI.53504 ( $\delta^{15}\text{N}$ :  
193 48.09‰,  $\delta^{15}\text{N}^{\alpha}$ : 1.71‰,  $\delta^{15}\text{N}^{\beta}$ =94.44‰,  $\delta^{18}\text{O}$ : 36.01‰) (provided by J. Mohn, EMPA; e.g. Mohn et al., 2014). The gases  
194 were calibrated on the Tokyo Institute of Technology scale for bulk and site-specific isotopic composition (Ostrom et al., 2018;  
195 Sakae Toyoda et al., 1999). Ratios of m/z 45/44, 46/44 and the 31/30 signals were used to calculate values of  $\delta^{15}\text{N}^{\text{bulk}}$   
196 (referenced against AIR-N<sub>2</sub>),  $\delta^{18}\text{O}$  (referenced against V-SMOW), and site-specific  $\delta^{15}\text{N}^{\alpha}$ ,  $\delta^{15}\text{N}^{\beta}$  based on Frame and Casciotti  
197 (2010) . Site preference (SP) was calculated as  $\delta^{15}\text{N}^{\alpha} - \delta^{15}\text{N}^{\beta}$  (Sutka et al., 2006; Toyoda and Yoshida, 1999).

## 198 **2.4. Pourbaix diagram**

199 In order to predict the stability and behaviour of the N- and Fe(II)-bearing chemical species in the same system, a Pourbaix  
200 (Eh-pH) diagram was constructed (Delahay et al., 1950) as a valuable tool to predict possible reactions and speciation of end  
201 products under different experimental conditions. To calculate the electrochemical potentials for the stepwise reduction of  
202 nitrite during denitrification, as well as Fe(II) oxidation reactions, standard electrode potentials were taken from different  
203 references (Table S1). The Pourbaix diagram presented in the discussion was devised using concentrations measured during  
204 the experiments performed for this study.

205 3. Results

206 3.1. Chemodenitrification kinetics



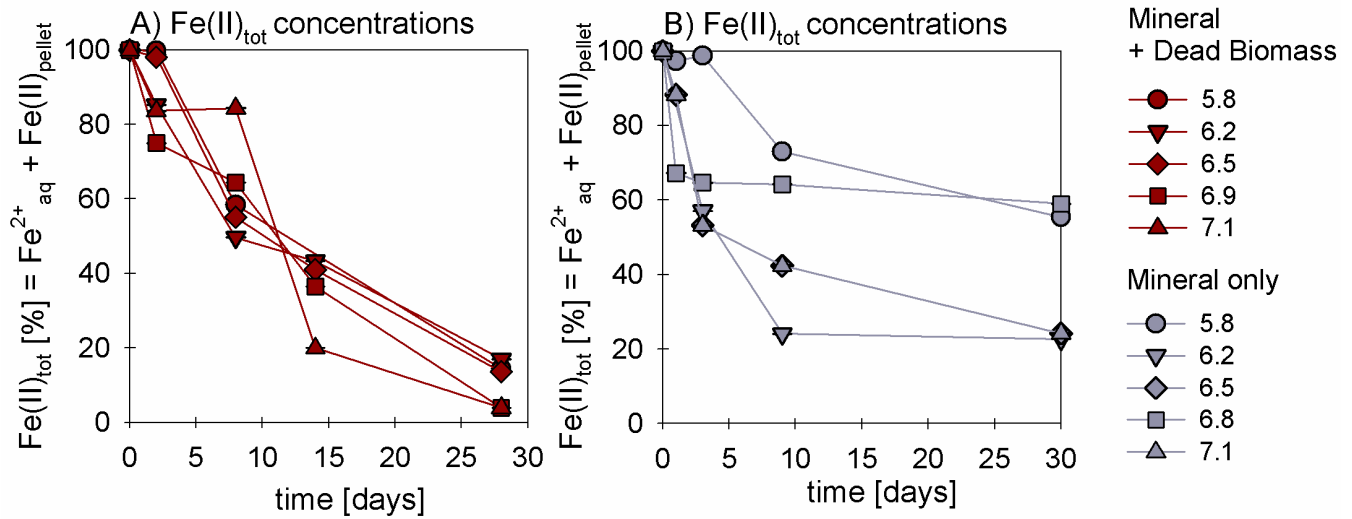
207  
208 **Figure 1: Nitrite reduction (A, C) and N<sub>2</sub>O production (B, D) over time in the mineral + dead biomass (red) and mineral-only (grey)**  
209 **setups over time and at different pH. Please note that at pH 5.8 twice the amount of nitrite was accidentally introduced. Standard**  
210 **error calculated from biological replicates (n = 9) is represented by the error bars.**

211  
212 In the presence of DB, NO<sub>2</sub><sup>-</sup> reduction rates were much higher compared to the mineral-only setup (Figure 1 A, C), with up to  
213 ~60% of the initially amended NO<sub>2</sub><sup>-</sup> being transformed during the incubation period, independent of the pH. The addition of  
214 DB led to a decrease in NO<sub>2</sub><sup>-</sup> concentrations from 2 mM to ~0.7 mM (Figure 1 A). The pH 5.8 treatment (unintentionally  
215 amended with 2x NO<sub>2</sub><sup>-</sup>) also showed a similar fractional reduction. In the mineral-only setups the decrease in NO<sub>2</sub><sup>-</sup>  
216 concentration was rather moderate and ranged between 0.3 (pH 7) and 0.1 mM (at lower pH) (Figure 1 C). In all treatments,  
217 N<sub>2</sub>O was produced but accounted for a maximum of only 0.7% of the NO<sub>2</sub><sup>-</sup> consumed. The final N<sub>2</sub>O yield per mole NO<sub>2</sub><sup>-</sup>  
218 reduced tended to be lower in the mineral plus DB versus the mineral-only amended setups for most of the pH (Figure 1 B vs.  
219 D). Highest N<sub>2</sub>O production was observed at circumneutral pH (7.1) in the mineral-only setup, while maximum final N<sub>2</sub>O



220 concentrations were observed at lower pH (6.2) in the incubations with DB (Figure 1 B; S4). A systematic pH effect, however,  
 221 could not be discerned.  $\text{Fe(II)}_{\text{total}}$  concentrations rapidly decreased in both setups. In the presence of DB,  $\text{Fe(II)}_{\text{total}}$  oxidation  
 222 was almost complete (Figure 2A), independent of the pH, whereas in the mineral-only experiment,  $\text{Fe(II)}_{\text{total}}$  decreased during  
 223 the first 5-10 days but then seemed to reach a steady state (Figure 2 B). At pH 6.8 and 5.8, only 40% of the  $\text{Fe(II)}_{\text{total}}$  was  
 224 oxidized, whereas at the other pH up to 80% of the  $\text{Fe(II)}_{\text{total}}$  initially amended was oxidized. Total Fe decreased over time  
 225 (Figure S2).

226



227

228 **Figure 2: Oxidation of total Fe(II) over time given (reported as % of initial concentration) in the mineral + dead biomass amended**  
 229 **(red) and the mineral-only setup (grey), tested at different pH. Standard error calculated from biological replicates (n = 9) is**  
 230 **represented by the error bars.**

231

232 Average rates for  $\text{NO}_2^-$  reduction and  $\text{N}_2\text{O}$  production at pH 6.8 were calculated (Table 1). Rates were calculated per day and  
 233 again these results emphasize that the amendment of dead biomass increased the rates by ~92%. Although not complete, Fe(II)  
 234 oxidation in the presence of DB was also more pronounced leading to only  $10.5 \pm 2.8\%$  Fe(II) remaining compared to the  
 235 mineral-only setup in which  $37.1 \pm 8.2\%$  Fe(II) remained. To complement the colorimetric data,  $^{57}\text{Fe}$  Mössbauer spectroscopy  
 236 was performed and data are presented in detail in the next section.

237

238

239

240

241

242

243

244  
245  
246  
247  
248  
249  
250  
  
  
  
  
  
  
  
  
  
251  
252  
  
253  
  
254  
255  
256  
257  
258  
259  
260  
261  
262  
263  
264  
265  
266  
267  
268  
269

**Table 1: Chemodenitrification kinetics and mineral transformation during mineral + dead biomass as well as the mineral only experiments.  $T_{ini}$  values represent means calculated by summarizing results across all pH  $\pm$  standard error. Overall reduction/production rates are calculated by subtracting  $\overline{[C]}_{t_0} - \overline{[C]}_{t_{end}} \pm \text{standard error} / \overline{[C]}_{t_{end}} - \overline{[C]}_{t_0} \pm \text{standard error}$ , respectively and are given per day. Fe(III) values are calculated by using  $^{57}\text{Fe}$  Mössbauer spectroscopy data. Mineral phases were also identified by using  $^{57}\text{Fe}$  Mössbauer spectroscopy with spectra collected at 77 K. Mineral-only sample taken after 28 days was inadvertently destroyed prior to Mössbauer measurement.**

	Mineral + Dead Biomass	Mineral-only
<b>NO<sub>2</sub><sup>-</sup> reduction (<math>\bar{X}</math>)</b>	0.053 $\pm$ 0.013 mmol L <sup>-1</sup> day <sup>-1</sup>	0.004 $\pm$ 0.003 mmol L <sup>-1</sup> day <sup>-1</sup>
<b>N<sub>2</sub>O production (<math>\bar{X}</math>)</b>	353.50 $\pm$ 32.91 nmol L <sup>-1</sup> day <sup>-1</sup>	204.02 $\pm$ 60.29 nmol L <sup>-1</sup> day <sup>-1</sup>
<b>Fe(II)<sub>total</sub> remaining (<math>\bar{X}</math>)</b>	10.54 $\pm$ 2.77%	37.08 $\pm$ 8.23%
<b>Fe(III) after NO<sub>2</sub><sup>-</sup> addition</b>	7.4%	9.9%
<b>Fe(III) after 28 days</b>	48.7%	*
<b>Mineral phase <math>t_{ini}</math></b>	Vivianite	Vivianite
<b>Mineral phase <math>t_{end}</math></b>	Vivianite/Ferrihydrite	*

\* Mössbauer sample processing failed

### 3.2. Fe mineral analysis

$^{57}\text{Fe}$  Mössbauer spectroscopy was used to quantify structural Fe(II) and Fe(III) contents of the samples and identify differences in mineralogy under the different reaction conditions. The hyperfine parameters of the mineral phases in in the mineral-only setup at  $t_{initial}$  (pH 6.84) are dominated by Fe(II) doublets (Figure 3 A, QSD Sites 1 and 2), which most closely match that of a vivianite spectrum (Muehe et al., 2013; Veeramani et al., 2011). There is a small component with low centre shift and quadrupole splitting, indicative of Fe(III), which accounts for ~10% of the spectral area (Figure 3 A, QSD Site 3). This suggests some minor oxidation occurred, potentially during transfer of sample into the spectrometer. The mineral phases in the DB-amended setup at  $t_{initial}$  (pH 6.89) shows very close approximation to the abiotic mineral-only setup, though with slightly less Fe(III) (~7.5% of the spectral area) (Figure 3 B, QSD Site 2). Precipitates analysed at the end of the DB-amended experiment (Day 28) show that at pH 6.89, the vivianite phase still dominates (Figure 3 C, QSD Sites 1 and 2), however, the Fe(III) component is now much more prominent (Figure 3 C, QSD Site 3), and suggests the formation of a poorly crystalline/short-ranged ordered mineral such as ferrihydrite (Cornell and Schwertmann, 2003). At the lowest pH (5.78) and in the presence of DB, the pattern of the precipitates is completely dominated by one doublet (Figure 3 C, QSD Site 1), with hyperfine parameters corresponding to a poorly ordered Fe(III) mineral such as ferrihydrite (Cornell and Schwertmann, 2003). Unfortunately, the sample processing failed for the mineral-only sample taken after 28 days and can therefore not be used for further elucidations. Detailed fitting results of the  $^{57}\text{Fe}$  Mössbauer spectroscopy are provided in Table 2.

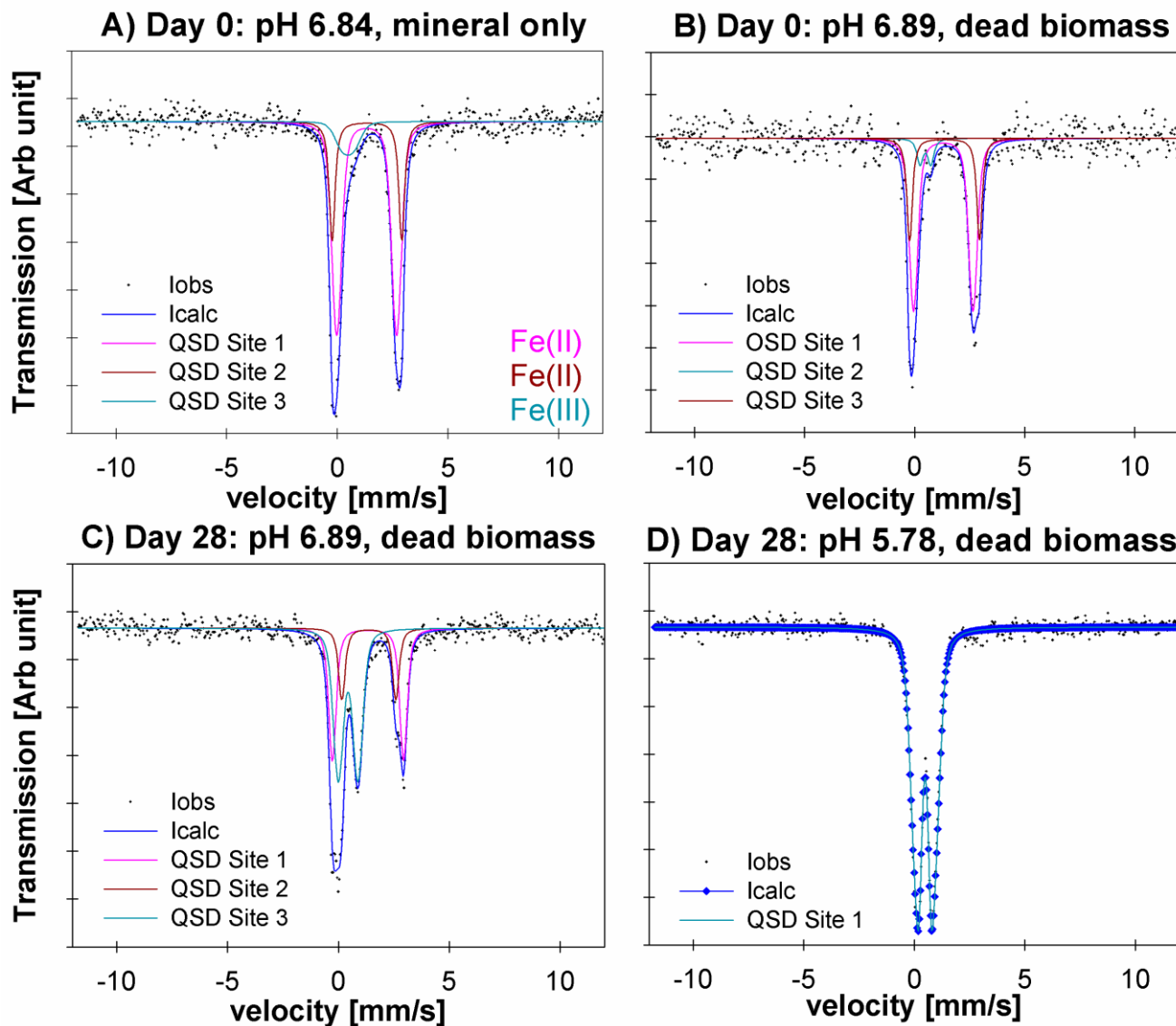


**Figure 3:**  $^{57}\text{Fe}$  Mössbauer spectra collected at 77 K for (A) the mineral only setup precipitates at day 0 and pH 6.84, (B) the mineral + dead biomass amended setup precipitates at day 0 at pH 6.89, (C) the mineral + dead biomass amended setup precipitates at day 28 and (D) the mineral + dead biomass amended setup precipitates at day 28 at pH 5.78. Full lines represent the calculated spectra and their sums. Colours of the fits represent the corresponding Fe phase and thus vary between the graphs: Fe(II) doublets (A, C – QSD Sites 1 and 2, B – QSD Sites 1 and 3) closely match the spectra known for vivianite. Minor amounts of Fe(III) are present at day 0 in both, the mineral-only and DB-amended setups (A/B QSD Site 3/2). Single doublets shown in C (QSD Site 3) and D (QSD Site 1) correspond to a poorly ordered Fe(III) mineral such as ferrihydrite.

282 **Table 2: Fitting results of Mössbauer spectroscopy. CS – centre shift, QS – quadrupole splitting, R.A. – Relative abundance**  
 283 **determined by integration under the curve, Chi<sup>2</sup> – goodness of fit; sample collection took place at t<sub>ini</sub> – initial time point and t<sub>end</sub> –**  
 284 **end time point; MO = mineral-only, MDB = mineral + dead biomass.**

Sample	Temp	Phase	CS	QS	R.A.	Error	Chi <sup>2</sup>
	[K]		[mm/s]	[mm/s]	[%]		
MO_pH6.8_t <sub>ini</sub>	77	Fe(II)	1.32	2.71	66.0	23.0	0.55
		Fe(II)	1.33	3.15	24.0	23.0	
		Fe(III)	0.47	0.63	9.9	4.8	
MDB_pH6.8_t <sub>ini</sub>	77	Fe(II)	1.30	2.70	65.0	14.0	0.68
		Fe(III)	0.49	0.49	7.4	3.6	
		Fe(II)	1.36	3.18	28.0	15.0	
MDB_pH6.8_t <sub>end</sub>	77	Fe(II)	1.33	3.21	34.3	2.4	0.73
		Fe(II)	1.37	2.44	17.0	2.8	
		Fe(III)	0.44	0.89	48.7	2.4	
MDB_pH5.8_t <sub>end</sub>	77	Fe(III)	0.49	0.79	100.0		0.66

285

286 **3.3. Nitrite and N<sub>2</sub>O isotope dynamics**

287 In experiments with DB, the δ<sup>15</sup>N-NO<sub>2</sub><sup>-</sup> and δ<sup>18</sup>O-NO<sub>2</sub><sup>-</sup> values showed a very consistent initial ~3-4‰-decrease (from -26‰  
 288 to -30‰ for δ<sup>15</sup>N and from ~+3‰ to 0‰ for δ<sup>18</sup>O) (Figure 4 A, B). After 5 days, the δ<sup>15</sup>N values started to increase again with  
 289 decreasing NO<sub>2</sub><sup>-</sup> concentrations, reaching final values of ~ -20‰ (Figure 4 A), whereas the concomitant increase in the δ<sup>18</sup>O-  
 290 NO<sub>2</sub><sup>-</sup> was much smaller (<1‰, Figure 4 B). The same pattern was observed for all pH levels. In mineral-only experiments,  
 291 isotope trends were quite different. In combination with far less consumption of NO<sub>2</sub><sup>-</sup>, the δ<sup>15</sup>N-NO<sub>2</sub><sup>-</sup> values decreased  
 292 throughout the entire abiotic experiment (Figure 4 C). In contrast, the δ<sup>18</sup>O-NO<sub>2</sub><sup>-</sup> first dropped by 2‰, reaching a clear  
 293 minimum of ~0.5 to -0.5 ‰, before rapidly increasing again. Over the remaining 25 days, the δ<sup>18</sup>O-NO<sub>2</sub><sup>-</sup> slowly decreased  
 294 reaching final values of ~1‰ (Figure 4 D) – similar to that of the mineral plus DB treatment.

295

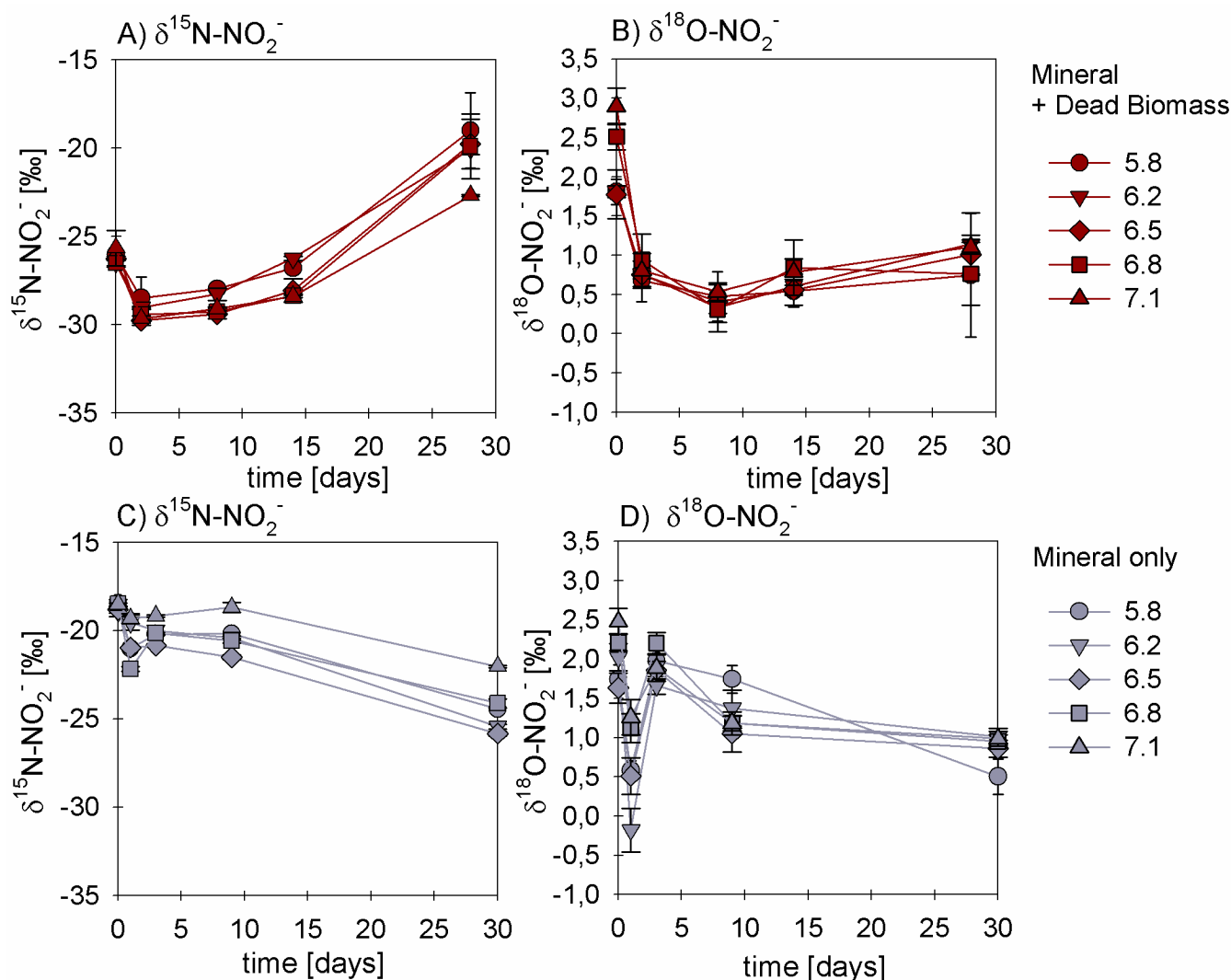
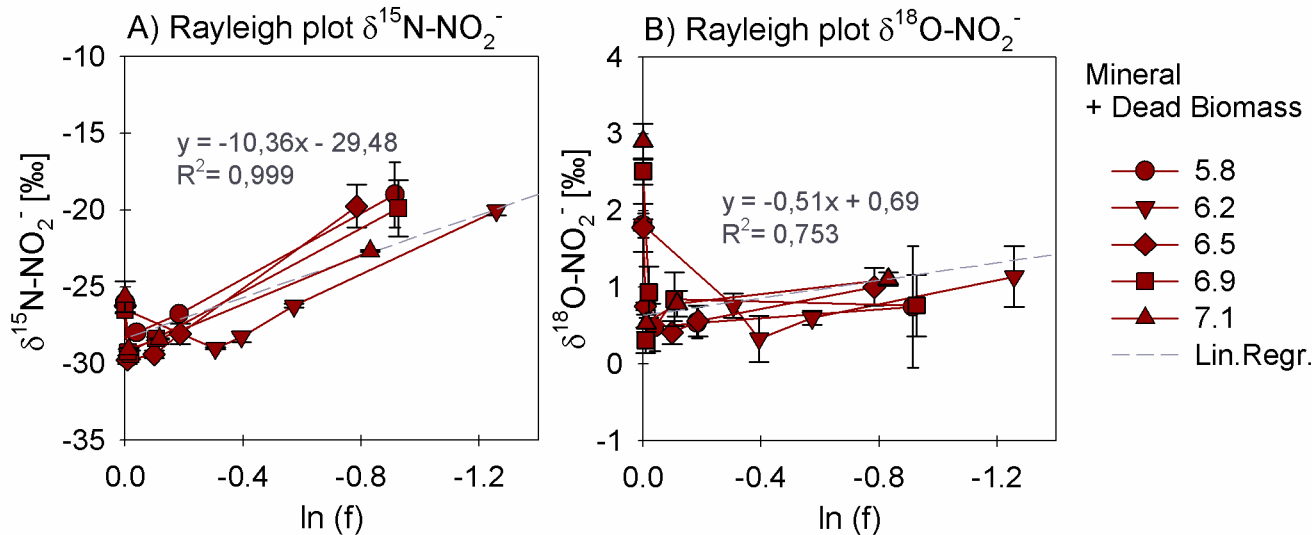


**Figure 4:**  $\delta^{15}\text{N}$  (A, C) and  $\delta^{18}\text{O}$  (B, D) values for  $\text{NO}_2^-$  measured in the mineral + dead biomass amended (red) and the mineral-only (grey) setups over time and at different pH. Standard error calculated from biological replicates (n = 3) is represented by the error bars.

In order to estimate the net N and O isotope fractionation for putative  $\text{NO}_2^-$  reduction (in the DB-amended experiments, where we observed a clear decrease in  $\text{NO}_2^-$ ), we plotted the  $\text{NO}_2^-$   $\delta^{15}\text{N}$  and  $\delta^{18}\text{O}$  values against the natural logarithm of the concentration of the residual  $\text{NO}_2^-$  (Rayleigh plot), where the slope of the regression line approximates the N and O isotope effects, respectively (Mariotti et al., 1981). At least after the initial period, when the  $\text{NO}_2^-$   $\delta^{15}\text{N}$  markedly increased with decreasing  $\text{NO}_2^-$  concentrations, the N isotope data are more or less consistent with Rayleigh isotope fractionation kinetics. The slope of the regression line suggests an average N isotope effect of -10.4‰ (Figure 5 A). For the mineral-only setup, no N isotope effect could be calculated, but the observed  $\text{NO}_2^-$   $\delta^{15}\text{N}$  trend suggest a small inverse N isotope fractionation (Figure

4 C). Similarly, trends in  $\text{NO}_2^- \delta^{18}\text{O}$  of the DB experiments are not as obviously governed by normal Rayleigh fractionation dynamics, at least not during the initial period, when the  $\delta^{18}\text{O}$  decreased despite decreasing  $\text{NO}_2^-$  concentrations. Considering the  $\delta^{18}\text{O}$  values only after 2 days of the incubation, the Rayleigh plot revealed an average O isotope enrichment factor of -0.5 ‰ (Figure 5 B), much lower than for N. Similar to N, O-isotope Rayleigh plots for the mineral-only experiments (Figure S5) did not exhibit coherent trends, as the fractional  $\text{NO}_2^-$  depletion was minor and not consistent (mostly less than 10%). Again, the observed  $\delta^{18}\text{O}$  minimum at day 2 of the abiotic incubations suggests that processes other than normal kinetic fractionation during  $\text{NO}_2^-$  reduction were at work, which cannot be described with the Rayleigh model. If at all, the decreasing  $\delta^{18}\text{O}$  values after day 5 in the mineral-only experiments, accompanying the subtle decrease in  $\text{NO}_2^-$  concentration in at least some of the treatments, suggest a small apparent inverse O isotope effect associated with the net consumption of  $\text{NO}_2^-$ . Despite the different  $\text{NO}_2^- \delta^{18}\text{O}$  dynamics during the course of the experiment, the final  $\delta^{18}\text{O}$  of the residual nitrite was very similar in both experimental setups, and independent of the pH.

319



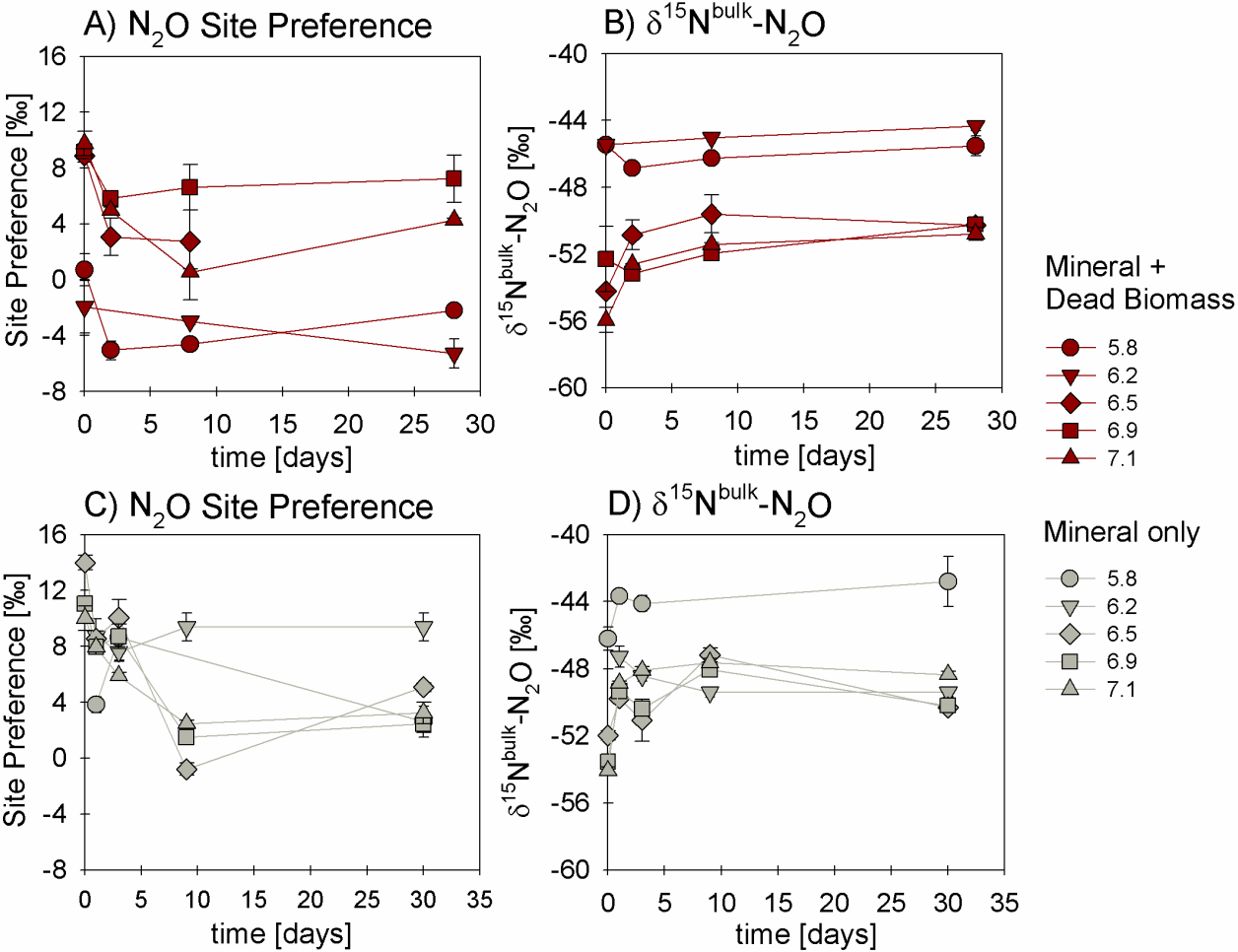
320

321 **Figure 5: Rayleigh plots for  $\text{NO}_2^- \delta^{15}\text{N}$  (A) and  $\delta^{18}\text{O}$  (B) values measured for the mineral + dead biomass amended setups over the**  
322 **ln of the substrate fraction remaining and at different pH. The average linear regression line was calculated starting with the lowest**  
323 **delta values (after the initial decrease in both  $\delta^{15}\text{N}$  and  $\delta^{18}\text{O}$  during the initial experimental phase). Equation and  $R^2$  are given in**  
324 **grey. Standard error calculated from biological replicates ( $n = 3$ ) is represented by the error bars.**

325

326 We also investigated the  $\text{N}_2\text{O}$  isotope dynamics during mineral-only and mineral plus DB incubations. Site preference (SP)  
327 and  $\delta^{15}\text{N}^{\text{bulk}}$  of the  $\text{N}_2\text{O}$  produced in both experimental setups were plotted over time (Figure 6 A and B) and show, except for  
328 a few values that require further investigation, almost no variation during the period of the experiment. Also, disregarding the  
329 rather high and unusual (but well replicated) values already mentioned, the majority of values obtained in both setups indicate  
330 that neither pH nor the amendment of DB seems to have had any influence on the isotopic composition of the produced  $\text{N}_2\text{O}$

331 (Figure 6 B vs. D). Over the course of the experiment,  $\delta^{15}\text{N}^{\text{bulk}}$   $\text{N}_2\text{O}$  values were around  $-50 \pm 6\text{‰}$ . SP was relatively low,  
 332 ranging roughly between  $-4$  and a maximum of  $+14\text{‰}$  (Figure 6 A, C), without any significant temporal change.  
 333



334  
 335 **Figure 6: Site Preference (SP; A, C) and  $\delta^{15}\text{N}^{\text{bulk}}$  (B, D) values of  $\text{N}_2\text{O}$  produced in experiments amended with mineral + dead biomass**  
 336 **(red) and mineral-only (grey). For pH 6.5, the final SP value (A) is missing due to analytical problems (overly large sample peak**  
 337 **areas). Standard error calculated from biological replicates (n = 3 or 2) is represented by the error bars.**

338  
 339 Rayleigh diagrams, in which  $\delta^{15}\text{N}^{\text{a}}$ ,  $\delta^{15}\text{N}^{\text{bulk}}$  and SP of the  $\text{N}_2\text{O}$  were plotted against concentrations of the reactant ( $\text{NO}_2^-$ )  
 340 remaining (Figure S6), confirm the similar  $\text{N}_2\text{O}$  isotope dynamics in the DB vs. mineral-only setups, despite the differential  
 341 degree of  $\text{NO}_2^-$  reduction (only minor in the mineral-only experiment, with f always greater 0.9) and despite the different  $\text{NO}_2^-$   
 342 N and O isotope dynamics. Similarly, the dual  $\text{N}_2\text{O}$   $\delta^{18}\text{O}$  vs.  $\delta^{15}\text{N}^{\text{bulk}}$  signatures (with the exception of two data points; Figure  
 343 S7) were almost equivalent in both setups, implying that, although modes of  $\text{NO}_2^-$  reduction clearly differ, a similar mechanism  
 344 of nitrite-reduction-associated  $\text{N}_2\text{O}$  production exists in both setups. The N and O isotopic results are summarized in Table 3  
 345 (see discussion).

## 346 4. Discussion and implications

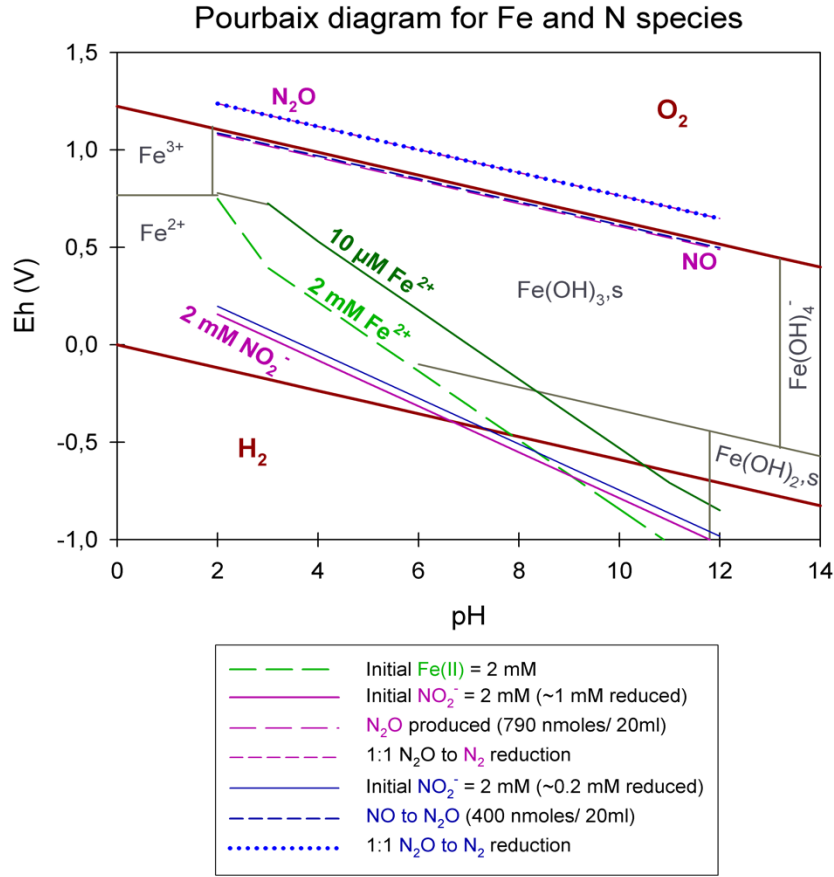
### 347 4.1. General evaluation of the abiotic reaction systematics

348 Overall, the abiotic reaction between  $\text{NO}_2^-$  and  $\text{Fe(II)}$ , heterogeneous or homogenous, has been considered thermodynamically  
349 favourable, and as major contributor to the global  $\text{N}_2\text{O}$  budget (e.g. Jones et al., 2015; Otte et al., 2019). Previous studies on  
350 abiotic  $\text{NO}_2^-$  reduction with  $\text{Fe(II)}$  have usually been performed in the presence of rather high concentrations ( $>2$  mM) of  $\text{NO}_2^-$   
351 and/or  $\text{Fe(II)}$ , without taking into account that chemodenitrification is in fact considered to be highly concentration-dependent  
352 (Van Cleemput and Samater, 1995). In addition, reaction dynamics were often tested under variable conditions including the  
353 presence of different  $\text{Fe(II)/Fe(III)}$  minerals, sediments, organic materials and/or bacterial cells (Chen et al., 2018; Grabb et  
354 al., 2017; Otte et al., 2019). Whether  $\text{NO}_2^-$  indeed acts as a direct oxidant of  $\text{Fe(II)}$  at circumneutral pH or whether the reaction  
355 requires catalysis is still a matter of debate (Kampschreur et al., 2011; Sorensen and Thorling, 1991).

356 Integrating concentrations that are pertinent to our experiments, we constructed a Pourbaix diagram (e.g. Delahay et al., 1950;  
357 Minguzzi et al., 2012) (Figure 7). Based on these (simplified) thermodynamic calculations, the abiotic reaction solely driven  
358 by the reaction of  $\text{NO}_2^-$  and aqueous  $\text{Fe}^{2+}$  at a pH range of 5 to 7 is not supported. Under our experimental conditions,  $\text{Fe}^{2+}$  is  
359 predicted to be oxidized by NO rather than  $\text{NO}_2^-$ . Considering Figure 7, an accumulation of NO at  $\mu\text{M}$  or even mM  
360 concentrations would result in a downward shift of the  $\text{NO}_2^-$  line. Therefore, an accumulation of NO would only lower the  
361 reactivity between  $\text{NO}_2^-$  and  $\text{Fe}^{2+}$ , which implies that  $\text{NO}_2^-$  is not oxidizing  $\text{Fe}^{2+}$ . Again, this also implies that the reactivity  
362 between  $\text{NO}_2^-$  and  $\text{Fe}^{2+}$  is only enhanced if NO concentrations are rather low (pM range). In order to avoid NO accumulation  
363 and thus to enhance the abiotic reaction between  $\text{NO}_2^-$  and  $\text{Fe}^{2+}$ , NO would need to react further (either with  $\text{Fe}^{2+}$  or otherwise).  
364 This would induce a reaction cascade, resulting in the constant reduction of  $\text{NO}_2^-$  and NO, and thus in higher  $\text{N}_2\text{O}$   
365 concentrations. In contrast, if NO does accumulate as previously reported, the reaction between  $\text{NO}_2^-$  and  $\text{Fe}^{2+}$  would be  
366 suppressed and only NO could be reduced further to  $\text{N}_2\text{O}$ , a reaction that of course also depends on gas equilibration dynamics  
367 occurring with the headspace of the system. Nevertheless, considering all these aspects, including the fact that the  $\text{N}_2\text{O}$   
368 produced corresponds only to a minor fraction of the initial  $\text{NO}_2^-$  reduced, NO acting as main oxidizing agent seems more  
369 likely. The reaction mechanisms in this system are, however, complex and we note that this simplified thermodynamic analysis  
370 does neglect catalytic effects that are possibly induced by reactive surfaces. The complexity of this system is further indicated  
371 by the fact that, according to the Pourbaix diagram, a pH response towards  $\text{N}_2\text{O}$  accumulation would be expected which has,  
372 however, never been reported so far. Furthermore, testing various pH did not reveal an obvious pH effect on the reaction  
373 dynamics. Changes in pH will most certainly affect interactions between species such as HNO,  $\text{NO}_2$  and  $\text{N}_2\text{O}$  and thus could  
374 impact the reaction dynamics. It appears that, for a more detailed understanding of this redox system, the  
375 reactants/intermediates involved and thus the specific reaction kinetics would need to be determined. Unfortunately,  
376 quantification of these intermediates is hampered by their high reactivity, transient nature, and lack of detection techniques  
377 that can be applied in batch culture experiments. Since low amounts (e.g., pM) of NO suffice to impact reaction dynamics and  
378 thus stimulate the reaction between  $\text{NO}_2^-$  and  $\text{Fe}^{2+}$ , NO quantification could be crucial to assess the environmental controls on



379 Fe(II)-coupled chemodenitrification. In laboratory biological denitrification experiments, accumulation of NO has been  
 380 reported (Goretski and Hollocher, 1988; Zumft, 1997) and was shown to even account for up to 40% of the initial  $\text{NO}_3^-$   
 381 amended (Baumgärtner and Conrad, 1992; Choi et al., 2006; Kampschreur et al., 2011; Ye et al., 1994; Zumft, 1997). Hence,  
 382 Kampschreur et al., (2011) concluded that chemodenitrification is not necessarily solely caused by a single-step reaction, and  
 383 proposed that the oxidation of  $\text{Fe}^{2+}$  is rather caused by a two-step mechanism. They observed an immediate formation and  
 384 accumulation of NO after  $\text{NO}_2^-$  was added to  $\text{Fe}^{2+}$ , and as soon as a considerable fraction of the  $\text{Fe}^{2+}$  was oxidized,  $\text{N}_2\text{O}$   
 385 formation was detected. Although NO and other possible intermediate (e.g.  $\text{NO}_2(\text{g})$ ) concentrations might not play a major  
 386 role with regard to mass balance considerations, their possible impact on the overall reaction systematics as well as the isotopic  
 387 fractionation, remains unclear.



388  
 389 **Figure 7: Pourbaix diagram depicting an Fe and N-species based system. Overall calculations are based on the Nernst equation using**  
 390 **values taken from literature (for equation and values see table S1). Green lines represent  $\text{Fe}^{2+}$  concentrations, pink lines represent**  
 391  **$\text{NO}_2^-$  reduction experiments, starting with 2 mM  $\text{NO}_2^-$ , resulting in the reduction of 1 mM  $\text{NO}_2^-$ , the production of 790 nmol /20 ml**  
 392  **$\text{N}_2\text{O}$  and a 1:1 transformation of  $\text{N}_2\text{O}$  to  $\text{N}_2$ ; blue lines represent  $\text{NO}_2^-$  reduction experiments, starting with 2 mM  $\text{NO}_2^-$ , resulting in**  
 393 **the reduction of 0.2 mM  $\text{NO}_2^-$ , the production of 790 nmol /20 ml  $\text{N}_2\text{O}$  and a 1:1 transformation of  $\text{N}_2\text{O}$  to  $\text{N}_2$ . Reduction/production**  
 394 **values were taken from our results presented in 3.1.**

## 395 4.2. Surface catalysis of chemodenitrification

396 Previous studies have shown that the initial presence of either Fe(III)(oxyhydr)oxides (Coby & Picardal, 2005; Klueglein &  
397 Kappler, 2013; Sorensen & Thorling, 1991) or amorphous Fe(II) minerals (Van Cleemput and Samater, 1995) can stimulate  
398 the abiotic reaction between  $\text{NO}_2^-$  and  $\text{Fe}^{2+}$ . As summarized in Table 1, under mineral-only conditions  $\text{NO}_2^-$  reduction was  
399 significantly lower ( $0.004 \pm 0.003 \text{ mmol L}^{-1} \text{ day}^{-1}$ ) than in identical experiments containing DB, which substantially enhanced  
400  $\text{NO}_2^-$  reduction ( $0.053 \pm 0.013 \text{ mmol L}^{-1} \text{ day}^{-1}$ ). The catalytic effect of Fe minerals on the abiotic  $\text{NO}_2^-$  reduction, which has  
401 been demonstrated before, seems to be amplified in the presence of DB. Relative to  $\text{NO}_2^-$  reduction rates, overall final  $\text{N}_2\text{O}$   
402 yields per mole  $\text{NO}_2^-$  reduced tended to be higher in the mineral-only setups. However, considering the initial  $\text{NO}_2^-$   
403 concentrations, only minor amounts of  $\text{N}_2\text{O}$  were produced in both setups, raising questions about the contribution of  
404 chemodenitrification to global  $\text{N}_2\text{O}$  emissions discussed by others (Grabb et al., 2017; Jones et al., 2015; Otte et al., 2019;  
405 Zhu-Barker et al., 2015). For example, in comparison to the  $\text{N}_2\text{O}$  yields in experiments where chemodenitrification was  
406 catalysed by green rust (up to 31%, Grabb et al., 2017), the amount of  $\text{N}_2\text{O}$  produced in our setups is far lower (<5% of the  
407 initial  $\text{NO}_2^-$ ).

408 Fe-bearing minerals are known for their high reactivity, ability to complex ligands (metals, humics) and phosphates, and  
409 surface protonation capacity via the sorption of  $\text{OH}^-$  groups (Elsner et al., 2004; Stumm and Sulzberger, 1992). Surface  
410 catalytic effects may include *direct* and *indirect* sorption-induced catalysis. In the environment, pH has been shown to have a  
411 strong influence on these sorption capacities of Fe minerals in general (Fowle and Konhauser, 2011). Considering the point of  
412 zero charge (PZC) of vivianite, which is with 3.3 below the lowest tested pH in our experiments, the mineral surface is  
413 positively charged under our experimental conditions (Luna-Zaragoza et al., 2009). Hence the pH range tested here will not  
414 affect the surface charge, and  $\text{NO}_2^-$  sorption onto mineral surfaces and corresponding heterogeneous reactions are possible. In  
415 contrast, cell surfaces are considered to be negatively charged (Wilson et al., 2001) and therefore might induce different effects  
416 than mineral surfaces. The charge of the cell surface most likely remained negative even after autoclaving (see e.g. Halder et  
417 al., 2015). Our results imply that the systematics of chemodenitrification are strongly dependent on the surface provided and  
418 that, depending on the availability and quality of catalytic surfaces, Fe coupled chemodenitrification may be a single-step  
419 reaction (between  $\text{NO}_2^-$  and Fe) or may occur in multiple steps (reaction between Fe and  $\text{NO}_2$ , as well as Fe and NO). As a  
420 consequence, the nature of surface catalysis would likely have a strong impact on the  $\text{N}_2\text{O}$  yield per mole  $\text{NO}_2^-$  reduced to NO.  
421 Since NO has been demonstrated to have a strong affinity towards  $\text{Fe}^{2+}$  and  $\text{Fe}^{3+}$  centres resulting in the formation of  $\text{Fe}^{x+}(\text{NO})_n$   
422 nitrosyls and thus triggering an enhancement of the  $\text{N}_2\text{O}$  decomposition rate (e.g. Rivallan et al., 2009). It remains unclear to  
423 what extent, and why, the quality of the catalytic surfaces plays a role. Particularly in the presence of organics and/or dead  
424 bacterial cells, which are known to have a high affinity to bind metal ions (e.g.  $\text{Ni}^{2+}$ ,  $\text{Cu}^{2+}$  or  $\text{Zn}^{2+}$ ), either directly or by  
425 forming surface complexes with hydroxyl groups (Fowle and Konhauser, 2011), a surface-catalysis-induced reaction can be  
426 expected. Besides acting as a catalyst via a reactive surface, the dead biomass might also have directly triggered the reaction.  
427 For example, non-enzymatic NO formation was studied and modelled by Zweier et al. (1999), suggesting that at concentrations

428 between 100 and 1000  $\mu\text{M}$ , abiotic  $\text{NO}_2^-$  disproportionation and thus NO formation at circumneutral pH in organic tissue is  
 429 still possible (Zweier et al., 1999). Furthermore, autoclaving might have ruptured cell walls and released organic compounds.  
 430 In the presence of phenolic compounds, humic substances, and other organic compounds,  $\text{NO}_2^-$  has been shown to form NO  
 431 via self-decomposition (Nelson and Bremner, 1969; Stevenson et al., 1970; Tiso and Schechter, 2015). Whether this may have  
 432 been the case also in our experiments remains unclear, since we did not conduct experiments containing only DB and  $\text{NO}_2^-$ .  
 433 Another possible consideration is the presence of extracellular polymeric substances (EPS), which should also be tested in  
 434 future studies. Liu et al., (2018) investigated nitrate-dependent Fe(II) oxidation with *Acidovorax* sp. strain BoFeN1, showing  
 435 that *c*-cytochromes were present in EPS secreted which could indeed act as electron shuttling agents involved in electron  
 436 transfer supporting chemolithotrophic growth. Since *S. oneidensis*, our model organisms used as DB supply, is known to  
 437 produce large amounts of EPS, harbouring *c*-cytochromes (Dai et al., 2016; Liu et al., 2012; White et al., 2016), a potential  
 438 impact of EPS on the reaction between  $\text{NO}_2^-$  and Fe(II) needs to be considered. However, possible cytochromes present in the  
 439 EPS most likely lost their activity due to protein denaturation during autoclaving (Liu & Konermann, 2009; Tanford, 1970).  
 440 Nevertheless, EPS is still present and can act as a catalysing agent to the abiotic reaction mechanism (Klueglein et al., 2014;  
 441 Nordhoff et al., 2017).  
 442 Fe(II)<sub>total</sub> oxidation via  $\text{NO}_2^-$  has also been observed in the mineral-only setups, but to a lower extent. Hence, the vivianite  
 443 mineral surfaces themselves seem to catalyse the abiotic reaction between  $\text{NO}_2^-$  and Fe(II)/  $\text{Fe}^{2+}$  (in parts, the stimulation of  
 444 Fe-dependent nitrite reduction may also be attributed vivianite dissolution providing ample Fe(II) substrate). Previous studies  
 445 reported on mineral-enhanced chemodenitrification (Dhakal et al., 2013; Grabb et al., 2017; Klueglein & Kappler, 2013;  
 446 Rakshit et al., 2008), and the catalytic effect may be due to  $\text{NO}_2^-$  adsorption onto the minerals surface possibly facilitating a  
 447 direct electron transfer. Similar findings have been reported previously on Fe(II) oxidation promoted by electron transfer  
 448 during adsorption onto a Fe(III) minerals surface (Gorski and Scherer, 2011; Piasecki et al., 2019).  $\text{OH}^-$  adsorption is probably  
 449 enabled by the minerals positive surface charge at  $\text{pH} > 6$ , resulting in a limited reactive surface availability. Complexation of  
 450 dissolved  $\text{Fe}^{2+}$ , which is provided by mineral dissolution, by  $\text{OH}^-$  groups would thus result in a lower overall  $\text{NO}_2^-$  reduction  
 451 rate compared to the DB-amended setups. Nevertheless, the NO formed by the initial  $\text{NO}_2^-$  reduction could, at still elevated  
 452  $\text{Fe}^{2+}$  levels, proceed until both dissolved and adsorbed Fe(II) is quantitatively oxidized to surface-bound Fe(III) (Kampschreur  
 453 et al., 2011). This would ultimately lead to similar Fe(II)<sub>total</sub> oxidation and  $\text{N}_2\text{O}$  production (and thus higher  $\text{N}_2\text{O}$  yields) as in  
 454 the DB amended experiment and thus explain the similar results.

### 455 **4.3. Mineral alteration during Fe-coupled chemodenitrification**

456 We used  $^{57}\text{Fe}$  Mössbauer spectroscopy in order to determine, whether the catalytic effects that enhanced chemodenitrification  
 457 with  $\text{Fe}^{2+}$  also modulated mineral formation. In both setups, addition of  $\text{Fe(II)Cl}_2$  to the 22 mM bicarbonate buffered medium  
 458 led to the formation of vivianite, an Fe(II)-phosphate. Shortly after the addition of  $\text{Fe}^{2+}_{\text{aq}}$ , the mineral phase in both setups was  
 459 dominated by Fe(II), but a small fraction of Fe(III) was also present. Initial fractions of Fe(III) were similar in both the mineral-  
 460 only and DB-amended experiments (9.9% and 7.4%, respectively) and, if not an artefact of Mössbauer sample handling, might

therefore have stimulated Fe(II) adsorption and oxidation (Gorski and Scherer, 2011; Piasecki et al., 2019). The reduction of  $\text{NO}_2^-$  was accompanied by a marked increase of Fe(III), likely in the form of short-range ordered ferrihydrite or lepidocrocite. Thus, the Fe(III) phase detected at day 0 most likely formed immediately after  $\text{NO}_2^-$  addition. This is supported by prior studies, which demonstrated the initiation of Fe(II) oxidation with  $\text{NO}_2^-$  within a short period of time (Jamieson et al., 2018; Jones et al., 2015). At the end of the DB experiment at pH 6.89, oxidized Fe(III) (most likely in the form of poorly ordered ferrihydrite) contributed 48.7% to the total Fe phases, with vivianite accounting for the remaining spectral area. Unfortunately, we are unable to compare the results of the DB-amended precipitates at the end of the experiment to the mineral-only setup, since the sample processing failed. Minerals obtained from the enrichment culture KS were mostly vivianite and ferrihydrite, which is, however, attributed to the fact that for the cultivation of the KS culture a high-phosphate medium is used (Nordhoff et al., 2017). In the abiotic experiments (10 mM Fe(II) and 10 mM  $\text{NO}_2^-$ ) presented by Jones et al., (2015), the formation of lepidocrocite, goethite and two-line ferrihydrite were observed after 6 to 48 hrs. In the experiments presented here, besides a short-range ordered Fe(III) phase, likely ferrihydrite, no other mineral phases could be identified after 28 days. Iron analysis also indicates that the oxidation of the  $\text{Fe(II)}_{\text{total}}$  went to completion at pH 5.8 whereas at pH 6.8, 52.3% of the  $\text{Fe(II)}_{\text{total}}$  remained at the end of the incubation experiment, resulting in the formation of a poorly-ordered ferrihydrite. Unfortunately, we did not measure the zeta potential of the starting solutions, which would probably help to explain the differences detected. We note that, although  $^{57}\text{Fe}$  Mössbauer spectroscopy was used to measure the Fe(II)/Fe(III) in the precipitates, the reported  $\text{Fe(II)}_{\text{total}}$  concentrations reflect the total Fe(II), i.e., of both the dissolved pellet (structurally-bound or adsorbed) and the aqueous  $\text{Fe}^{2+}$  in the supernatant measured by ferrozine. The results obtained by Mössbauer analysis (50% Fe(II) remaining) seem to contradict the ferrozine assay (<10% remaining) (see Table 1 and 2). The presence of ferrous Fe, either as structurally-bound Fe(II) or adsorbed  $\text{Fe}^{2+}$  does indeed play a crucial role with regards to the reaction dynamics occurring at the mineral surfaces, particularly if we assume that N-reactive species are also still present (Rivallan et al., 2009). In addition, the initially formed Fe(III) phase might also induce another feedback to the N and even the Fe cycle since Fe(III) minerals are also highly reactive (Grabb et al., 2017; Jones et al., 2015). Mineral structure and thus Fe(II) location within the lattice can influence the overall Fe accessibility, the binding site at the mineral surface and thus overall reactivity (Cornell and Schwertmann, 2003; Luan et al., 2015; Schaefer, 2010). If the initial formation of Fe(III), however, enhanced the reaction between  $\text{NO}_2^-$  and Fe(II), similar results in both setups should have been observed, which this was not the case since  $\text{NO}_2^-$  reduction patterns in the mineral-only experiments were much lower. This also indicates again, that the presence of DB indeed contributed greatly to the reaction in the DB experiments. Furthermore, results obtained from Mössbauer analysis are the only results supporting a pH-dependent effect: At pH 5.78 and in the presence of DB, all vivianite was fully transformed into a short-range ordered Fe(III) phase whereas at pH 6.89, vivianite remained a major component. This presence of vivianite also indicates that no further Fe(II) oxidation occurred even though  $\text{NO}_2^-$  reduction was incomplete. The incomplete reduction of  $\text{NO}_2^-$  in turn suggests that further Fe(II) oxidation was limited due to blocked or deactivated reaction sites on mineral surfaces. Also, considering that at pH 5.8 and in the presence of DB, the initial  $\text{NO}_2^-$  concentrations were higher but the overall reaction

494 dynamics were quite similar to the other reaction conditions, the concentration dependency of the reaction between  $\text{NO}_2^-$  and  
495  $\text{Fe(II)}$  is again supported.

#### 496 **4.4. Nitrite and $\text{N}_2\text{O}$ N and O isotope dynamics during chemodenitrification**

497 In the presence of only vivianite, a decrease in  $\delta^{15}\text{N-NO}_2^-$  of  $\sim 3\text{‰}$  occurred in parallel with initially decreasing  $\text{NO}_2^-$   
498 concentrations. Initial  $\delta^{18}\text{O-NO}_2^-$  values also reflect this drop of  $3\text{‰}$  during the first 3 days but level off and stabilize at  $1\text{‰}$   
499 after 9 days. The initial decrease in both  $\delta^{15}\text{N}$  and  $\delta^{18}\text{O}$  of  $\text{NO}_2^-$  suggest apparent inverse isotope effects, which to the best of  
500 our knowledge have never been observed during chemodenitrification, and have only been reported for enzymatic  $\text{NO}_2^-$   
501 oxidation (Casciotti, 2009). Since biological  $\text{NO}_2^-$  oxidation can be ruled out (no  $\text{NO}_3^-$  produced, no microbes), the decrease  
502 in  $\delta^{15}\text{N-NO}_2^-$ , though subtle, could indicate that either heavy isotopes are incorporated in the products formed (i.e.  $\text{NO}$ ,  $\text{N}_2\text{O}$ ),  
503 at least at the beginning of the incubation period. Normally, the heavier isotopes build compounds with molecules of higher  
504 stability (Elsner, 2010; Fry, 2006; Ostrom & Ostrom, 2011). This is particularly true for the formation of some minerals or  
505 highly stable molecules that are formed under mineral-only conditions, where processes can reach an isotopic equilibrium (He  
506 et al., 2016; Hunkeler & Elsner, 2009; Li et al., 2011; Ostrom & Ostrom, 2011). However, in the system presented here, N  
507 incorporation into mineral phases can be excluded, hence another process must favour the heavy N-atoms. Since this initial  
508 drop in  $\delta^{15}\text{N}$  was also observed in the DB-amended experiments, a possible explanation might be that the isotope values here  
509 reflect the sorption or complexation mechanism of  $\text{NO}_2^-$  onto the reactive surfaces. In contrast  $\delta^{18}\text{O-NO}_2^-$  values, after the  
510 initial decrease, did not change greatly with decreasing  $\text{NO}_2^-$  concentrations. The stabilization of the  $\delta^{18}\text{O-NO}_2^-$  towards the  
511 end of the experiment most likely reflects the oxygen isotope equilibration between  $\delta^{18}\text{O-NO}_2^-$  and the  $\delta^{18}\text{O}$  of the water in the  
512 medium. Temporal  $\delta^{18}\text{O-NO}_2^-$  dynamics did not change greatly between the different pH treatments, and in all cases the final  
513  $\delta^{18}\text{O-NO}_2^-$  ranged between  $0.5$  and  $1\text{‰}$ . The kinetics of abiotic O-atom exchange is a function of temperature and pH. At near  
514 neutral pH, at room temperature, one can expect  $\text{NO}_2^-$  to be fully equilibrated after two to three days (Casciotti et al., 2007).  
515 At higher pH, the first order rate constants for the equilibration with water are lower (Buchwald and Casciotti, 2013), but  
516 equilibrium conditions should have been reached well within the incubation period. Indeed, the final  $\delta^{18}\text{O-NO}_2^-$  was consistent  
517 with an equilibrium O isotope effect between  $\text{NO}_2^-$  and  $\text{H}_2\text{O}$  with a  $\delta^{18}\text{O}$  of  $\sim -11.5\text{‰}$  (Buchwald and Casciotti, 2013). With  
518 regards to  $\delta^{15}\text{N-NO}_2^-$  values of the DB-amended experiments, a similar behaviour is found within the first 3 days (i.e., decrease  
519 in  $\delta^{15}\text{N}$ ), followed by a clear increase in  $\delta^{15}\text{N-NO}_2^-$  of  $\sim 10\text{‰}$ . While it is difficult to explain the initial decrease in  $\delta^{15}\text{N-NO}_2^-$   
520 (a feature that was not observed in other chemodenitrification experiments (i.e. Grabb et al., 2017; Jones et al., 2015), the  
521 subsequent increase in  $\delta^{15}\text{N}$  can be attributed to normal isotopic fractionation associated with chemodenitrification and an N  
522 isotope effect ( $-9\text{‰}$ ) that is consistent with those previously reported on Rayleigh-type N and O isotope kinetics during  
523 chemodenitrification with  $\text{Fe(III)}$ -bearing minerals such as nontronite and green rust (Grabb et al., 2017). In contrast,  $\delta^{18}\text{O-}$   
524  $\text{NO}_2^-$  values initially decrease as in the abiotic experiment but then level off faster reaching final values of  $\sim 1\text{‰}$ , again most  
525 likely explained by O atom isotope exchange pulling the  $\delta^{18}\text{O-NO}_2^-$  values towards the O-isotope equilibrium value. This value  
526 is given by the  $\delta^{18}\text{O}_{\text{H}_2\text{O}} + {}^{18}\epsilon_{\text{eq,NO}_2^-}$ , whereas the latter is defined as the equilibrium isotope effect between  $\text{NO}_2^-$  and  $\text{H}_2\text{O}$  and

has been shown to yield values of roughly +13‰ (Casciotti et al., 2007). Overall, it seems that the non-linear behaviour of the  $\text{NO}_2^-$  in the O isotope Rayleigh plot is most likely due to the combined effects of kinetic O isotope fractionation during  $\text{NO}_2^-$  reduction, and O atom exchange between  $\text{NO}_2^-$  and  $\text{H}_2\text{O}$ .

$\text{NO}_2^-$  N and O isotope trends observed under the DB-amended conditions (in which a large portion of the  $\text{NO}_2^-$  pool was consumed), somewhat contradict prior reports of chemodenitrification exhibiting a clear increase in both  $\delta^{15}\text{N}$  and  $\delta^{18}\text{O}\text{-NO}_2^-$ , with N isotope enrichment factors for  $\text{NO}_2^-$  reduction between -12.9 and -18.1‰ and an O isotope effect of -9.8‰ (Jones et al., 2015). Consistent with our data, however, they also observed that, at least in abiotic experiments where  $\text{NO}_2^-$  consumption is rather sluggish due to  $\text{Fe}^{2+}$  limitation (as a result of either oxidation or simply occlusion), O-isotope exchange isotope effects mask the effects of kinetic O isotope fractionation. While we cannot say at this point what exactly governs the combined  $\text{NO}_2^-$  N vs. O isotope trends in the two different experimental conditions, we observed that the two processes (water isotope equilibrium and KIE) competing with each other lead to different net dual isotope effects. Our data cannot resolve whether these observations reflect fundamental differences or simply changes in the relative proportion of the competing processes. Nevertheless, our observations may still be diagnostic for chemodenitrification catalysed by a mineral surface on the one hand, and Fe-coupled chemodenitrification that involves catalytic effects by dead bacterial cells on the other. The mineral catalyst evidently plays an important role with regards to chemodenitrification kinetics, reaction conditions, surface complexation or contact time between the  $\text{NO}_2^-$  substrate and the mineral phase (Samarkin et al., 2010), and in turn the combined kinetic/equilibrium N and O isotope effects.

The  $\Delta^{15}\text{N}$  values ( $\Delta^{15}\text{N} = \delta^{15}\text{N}_{\text{nitrite}} - \delta^{15}\text{N}_{\text{N}_2\text{O}}^{\text{bulk}}$ ) presented in Table 3 were obtained by subtracting the average  $\delta^{15}\text{N}^{\text{bulk}}$  value of  $\text{N}_2\text{O}$  (abiotic  $-49.5 \pm 0.6\text{‰}$ ; dead biomass  $-50.5 \pm 0.8\text{‰}$ ) across all pH and throughout the experiment from the average of the initial  $\delta^{15}\text{N}_{\text{nitrite}}$  value. These values can provide insight on reaction kinetics between  $\text{NO}_2^-$ , NO, and  $\text{N}_2\text{O}$  (Jones et al., 2015). In both setups there is an offset between the  $\text{NO}_2^-$  and  $\text{N}_2\text{O}$   $\delta^{15}\text{N}$ , which is clearly higher than what would be expected based on the  $\text{NO}_2^-$  reduction  $\text{NO}_2^-$  isotope effect of  $<10\text{‰}$ . Following the argumentation of Jones et al. (2015), who reported a similar N isotopic offset between  $\text{NO}_2^-$  and  $\text{N}_2\text{O}$  of  $27.0 \pm 4.5\text{‰}$ , this could be indicative for a heavy N accumulating in a forming NO pool, whereas  $^{14}\text{N}$  is preferentially reacting to  $\text{N}_2\text{O}$  or  $\text{N}_2$ , respectively. This might even be supported by the rather low  $\delta^{15}\text{N}^{\text{bulk}}$  values detected for  $\text{N}_2\text{O}$  in both setups.

561 **Table 3: Comparison of the isotope values obtained during dead biomass versus the abiotic experiments. t0 values represent means**  
 562 **calculated by summarizing results across all pH  $\pm$  standard error.  $\delta^{15}\text{N}$  and  $\delta^{18}\text{O}$  values were calculated using  $\bar{x}_{t0} - \bar{x}_{tend}$ , whereas**  
 563 **an overall increase from the initial value is marked with  $\uparrow$ , and a decrease with  $\downarrow$ . The calculated isotope fractionation factor ( $\epsilon$ ) is**  
 564 **based on the slope between the lowest initial value (here at t1) and tend for all pH.  $\Delta^{15}\text{N}$  ( $= \delta^{15}\text{N}_{\text{nitrite}} - \delta^{15}\text{N}_{2\text{O}}^{\text{bulk}}$ ) was calculated for**  
 565 **the end of the experiment.**

	Dead Biomass	Abiotic
$\delta^{15}\text{N}_{\text{nitrite}}(\text{t0-tend})$	$\uparrow 5.99 \pm 0.65\text{‰}$	$\downarrow 5.93 \pm 0.73\text{‰}$
$\delta^{18}\text{O}_{\text{nitrite}}(\text{t0-tend})$	$\downarrow 1.75 \pm 0.23\text{‰}$	$\downarrow 1.15 \pm 0.18\text{‰}$
$^{15}\epsilon_{\text{nitrite}}$	$-10.36 \text{‰}^{\#}$	-
$^{18}\epsilon_{\text{nitrite}}$	$-0.51\text{‰}^{\#}$	-
<b>SP</b>	$2.3 \pm 1.2\text{‰}$	$6.5 \pm 0.8\text{‰}$
$\delta^{15}\text{N}^a$	$-48.9 \pm 0.1\text{‰}$	$-46.3 \pm 0.06\text{‰}$
$\delta^{15}\text{N}^{\text{bulk}}$	$-50.5 \pm 0.8\text{‰}$	$-49.5 \pm 0.6\text{‰}$
$\Delta^{15}\text{N}$	$24.4\text{‰}$	$30.9\text{‰}$

566 <sup>#</sup> n=4 (t1 to tend); - concentrations in abiotic experiment fluctuate and show only minor decrease, hence  $^{15}\epsilon$  and  $^{18}\epsilon$  could not be calculated.  
 567

568 While our results clearly showed that N<sub>2</sub>O accumulates over the course of the reaction, it remains unclear, which additional  
 569 end products are present at the final stage of the experiment. If NO accumulates (instead of following the reaction cascade  
 570 further), the substrate-product relationship between the  $\delta^{15}\text{N}$ -NO<sub>2</sub><sup>-</sup> and  $\delta^{15}\text{N}$ -N<sub>2</sub>O values that would be expected in a closed  
 571 system is perturbed, leading to significantly higher  $\Delta^{15}\text{N}$  than predicted by the  $\delta^{15}\text{N}$ -NO<sub>2</sub><sup>-</sup> trend. Hence, the calculated  $\Delta^{15}\text{N}$  of  
 572 the mineral-only treatment (30.9‰) is slightly higher than that of the DB experiment (24.4‰), and would therefore suggest  
 573 that despite the differences in chemodenitrification kinetics (i.e. different NO<sub>2</sub><sup>-</sup> reduction rates and extent), the NO pool formed  
 574 is enriched in heavy N in both treatments, respectively. Alternatively, fractional reduction of the produced N<sub>2</sub>O to N<sub>2</sub> may also  
 575 affect the  $\Delta^{15}\text{N}$  since it would presumably increase the  $\delta^{15}\text{N}$ -N<sub>2</sub>O and thereby raise the low  $\delta^{15}\text{N}$ -N<sub>2</sub>O closer to the starting  
 576  $\delta^{15}\text{N}$ -NO<sub>2</sub><sup>-</sup>. Abiotic decomposition of N<sub>2</sub>O to N<sub>2</sub> in the presence of Fe-bearing zeolites has been investigated previously  
 577 (Rivallan et al., 2009), however, it remains unclear if this process could also occur here. Fractional N<sub>2</sub>O reduction is also not  
 578 explicitly indicated by the SP values, which would reflect an increase with N<sub>2</sub>O reduction (Ostrom et al., 2007; Winther et al.,  
 579 2018). The SP values in both mineral-only and DB-amended experiments were, with some exceptions, relatively low ( $6.5 \pm$   
 580  $0.8\text{‰}$ ;  $2.3 \pm 1.2\text{‰}$ ; Fig. 6, Table 3). In fact, SP values observed during the course of our experiments are significantly lower  
 581 compared to SP values reported in other studies on Fe-oxide-mineral associated chemodenitrification (e.g.  $\sim 16\text{‰}$ ; Jones et al.  
 582 (2015);  $26.5\text{‰}$ ; Grabb et al. 2017), or during the abiotic N<sub>2</sub>O production during the reaction of Fe and a NH<sub>2</sub>OH/NO<sub>2</sub><sup>-</sup> mixture  
 583 ( $34\text{‰}$ ; Heil et al. 2014). While the variety of different SP values for chemodenitrification-derived N<sub>2</sub>O suggests different  
 584 reaction conditions and catalytic effects, our SP data seem to imply that the mineral catalyst plays only a minor role with  
 585 regards to the isotopic composition of the N<sub>2</sub>O produced. However, since N<sub>2</sub>O concentrations, even if minor, are increasing  
 586 towards the end of the experiments, production and possible decomposition as well as ongoing sorption mechanisms might

587 also serve as possible explanation leading to these rather low SP values. N<sub>2</sub>O SP values have been used as valuable tracer for  
 588 microbial N<sub>2</sub>O production (Ostrom & Ostrom, 2012). Based on pure culture studies (Ostrom et al., 2007; Winther et al., 2018;  
 589 Wunderlin et al., 2013) and investigations in natural environments (Wenk et al., 2016) a SP range of -10 to 0‰ is considered  
 590 to be characteristic for denitrification or nitrifier-denitrification (Sutka et al., 2006; Toyoda et al., 2005), whereas higher values  
 591 are usually attributed to nitrification or fungal denitrification (Ostrom & Ostrom, 2012; Wankel et al., 2017; Well & Flessa,  
 592 2009). The SP values reported here (0 to 14‰) fall well within the range of biological N<sub>2</sub>O production, explicitly denitrification  
 593 and soil derived denitrification (2.3 to 16‰) (Ostrom & Ostrom, 2012), rendering the separation between chemodenitrification  
 594 and microbial denitrification based on N<sub>2</sub>O isotope measurements difficult, if not impossible.

595 In summary, the N and O isotope systematics of chemodenitrification are multifaceted, depending on the environmental  
 596 conditions, reaction partners provided, and/or the speciation of precipitated mineral phases. The systematics observed here are  
 597 clearly not entirely governed by normal kinetic isotope fractionation only, as has also been observed in previous work. Grabb  
 598 et al. (2017) demonstrated that there is a relationship between reaction rate and kinetic NO<sub>2</sub><sup>-</sup> N and O isotope effects, with  
 599 faster reaction leading to lower <sup>15</sup>ε and <sup>18</sup>ε. Again, changes in the expression and even in the direction of the isotope effects in  
 600 the NO<sub>2</sub><sup>-</sup> pool suggest that multiple processes, including equilibrium isotope exchange (at least with regards to the δ<sup>18</sup>O- NO<sub>2</sub><sup>-</sup>  
 601 ), are contributing to the net N and O isotope fractionation regulated by the experimental conditions and reaction rates. As  
 602 pointed out by Grabb et al. (2017), and as supported by our comparative study with pure abiotic mineral phases and with added  
 603 dead biomass, the accessibility of Fe(II) to the reaction may be a key factor regarding the degree of N and O isotope  
 604 fractionation expressed, particularly if complexation limits the reactive sites of the mineral. The conditions that, at least  
 605 transiently, lead to the apparent inverse N and O isotope fractionation observed here for chemodenitrification requires  
 606 particular attention by future work. At this point, we can only speculate about potential mechanisms, which are indicated in  
 607 the conceptual illustration (Figure 8). As chemodenitrification seems to be catalysed by reactive surfaces of Fe(II)/Fe(III)-  
 608 minerals and/or organics (including cells), sorption onto these surfaces might play a crucial role in the fractionation of N and  
 609 O isotopes. For example, during the catalytic hydrogenation of CO<sub>2</sub> on Fe and Co catalysts, a subtle depletion (ca. 4‰) in  
 610 <sup>13</sup>CO<sub>2</sub> at progressed conversion to methane has been explained by the precipitation of a <sup>13</sup>C-enriched carbon intermediate (e.g.,  
 611 CO-graphite) on the catalyst surface (Taran et al., 2010). We are fully aware that it is difficult to compare our system with  
 612 Fischer-Tropsch synthesis of methane occurring at high temperature and pressure. Yet given the indirect evidence for NO  
 613 accumulation in our experiments, it may well be that preferential chemisorption/complexation of “heavy” intermediate NO  
 614 occurs, which may lead to transient <sup>15</sup>N-depletion in the reactant NO<sub>2</sub><sup>-</sup> pool. Considering that the N<sub>2</sub>O concentrations measured  
 615 in our experiments were comparatively low and that δ<sup>15</sup>N<sup>bulk</sup>-N<sub>2</sub>O values did not noticeably change throughout the experiments,  
 616 it is unlikely that N<sub>2</sub>O is the final product, and formation of N<sub>2</sub> via abiotic interactions between NO<sub>2</sub><sup>-</sup> and NO is probably also  
 617 involved (Doane, 2017; Phillips et al., 2016). Indeed, if accumulated as the final product, the δ<sup>15</sup>N<sup>bulk</sup>-N<sub>2</sub>O value at the end of  
 618 the incubation should be ~-33‰ (according to closed-system accumulated-product Rayleigh dynamics), significantly higher  
 619 than what we measured (~ -50 ± 6 ‰). Hence, whether N<sub>2</sub>O is an intermediate or parallel side product, its role in the overall  
 620 reaction complicates N and O isotope mass balance dynamics in complex ways.



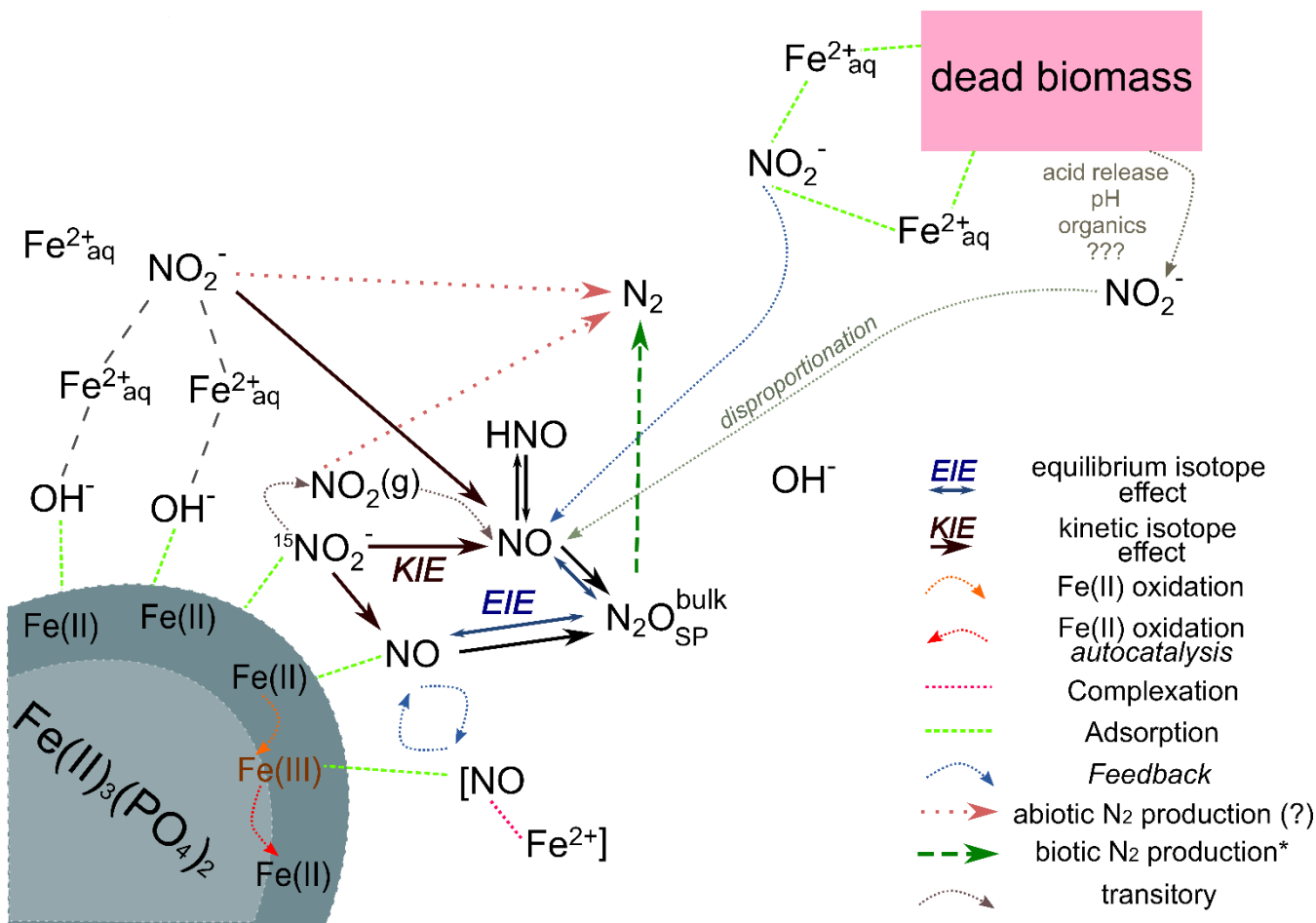


Figure 8: Conceptual figure depicting the proposed reaction mechanisms and feedbacks between the different N species during chemodenitrification induced by the presence of a mineral surface (lower left corner) or (dead) biomass (upper right corner). Adsorption of Fe<sup>2+</sup> (directly or via complexation by OH<sup>-</sup>) as well as NO<sub>2</sub><sup>-</sup> could catalyse a direct reaction between both. In addition, NO<sub>2</sub><sup>-</sup> adsorption onto the Fe(II) mineral might also induce disproportionation, leading to NO<sub>x</sub> formation. These formed intermediates, although transitory, may impact the overall reaction dynamics by e.g. complex formation (i.e. [NO-Fe<sup>2+</sup>]) or direct Fe(II) oxidation. The produced Fe(III) might induce another feedback loop (autocatalysis) resulting in further Fe(II) oxidation. Similar processes are possibly induced by the presence of (dead) biomass. Adsorption and complexation of either NO<sub>2</sub><sup>-</sup> and Fe<sup>2+</sup> would enhance the reaction between both. In addition, the presence of organic acids would decrease the pH locally and thereby promote and accelerate NO<sub>2</sub><sup>-</sup> disproportionation and thus additionally enhance Fe(II) oxidation. Our results suggest that NO<sub>2</sub><sup>-</sup> reduction results in an KIE, which should influence the isotopic composition of NO. N<sub>2</sub>O here is an intermediate, the isotopic composition of which is mainly influenced by an EIE between NO and N<sub>2</sub>O. The low N<sub>2</sub>O yields as well as the N<sub>2</sub>O isotopic results (bulk, SP) clearly suggests that N<sub>2</sub> is produced abiotically.

## 635 5. Conclusions and outlook

636 In the absence of any clear (genetic) evidence for enzymatic NDFeO from cultures (e.g. *Acidovorax* sp. strain BoFeN1),  
637 heterotrophic denitrification/ $\text{NO}_3^-$  reduction coupled to abiotic oxidation of Fe(II) with the  $\text{NO}_2^-$  has been presented as the most  
638 reasonable explanation for NDFeO. Here we investigated the second, abiotic step, clearly demonstrating that Fe-associated  
639 abiotic  $\text{NO}_2^-$  reduction can be catalysed by mineral and organic phases under environmentally relevant conditions, as found  
640 for example in soils and aquifers. Our results confirm that reactive surfaces play a major role with regards to the reaction  
641 between  $\text{NO}_2^-$  and Fe(II) and that surface-catalysed chemodenitrification appears to not only contribute to the production of  
642 the greenhouse gas  $\text{N}_2\text{O}$  in environments hosting active cycling of Fe and N, but also to an abiotic production of  $\text{N}_2$ . In order  
643 to understand the mechanistic details of Fe-coupled chemodenitrification, natural-abundance measurements of reactive-N  
644 isotope ratios may help distinguish between abiotic and biotic reactions during NDFeO. Our results, however, indicate that the  
645 potential of coupled N and O isotope measurements to determine the relative importance of Fe-induced N-transformations in  
646 natural environments is somewhat limited. Considering, for example, the apparent inverse N isotope effect in the mineral-only  
647 experiments, our studies show that the  $\text{NO}_2^-$  N vs. O isotope systematics seem to contrast distinctly between biotic and abiotic  
648  $\text{NO}_2^-$  reduction, potentially permitting the disentanglement of the biotic versus abiotic processes.  $\text{N}_2\text{O}$  SP values seem to be  
649 less diagnostic with regards to discriminating between chemodenitrification-derived  $\text{N}_2\text{O}$  and  $\text{N}_2\text{O}$  that is produced during  
650 microbial  $\text{NO}_2^-$  reduction. Our results suggest that both the reaction between Fe(II) and reactive N species, as well as the  
651 resulting isotope effects, are dependent on the reactive surfaces available. The presence of organic material seems to enhance  
652  $\text{NO}_2^-$  reduction and, to a lesser extent also  $\text{N}_2\text{O}$  production, leading to the enrichment in  $^{15}\text{N}$  in the residual  $\text{NO}_2^-$ , as predicted  
653 by Rayleigh-type kinetic N isotope fractionation. In the presence of only Fe(II) minerals,  $\text{NO}_2^-$  reduction rates are significantly  
654 lower, and net N and O isotope effects are not governed by kinetic isotope fractionation only, but also by isotope equilibrium  
655 fractionation during exchange with the ambient mineral phase and/or the ambient water (in the case of O isotopes). While  $\text{N}_2\text{O}$   
656 production was significant, the  $\text{N}_2\text{O}$  yields were below 5%, suggesting that a significant fraction of the  $\text{NO}_2^-$  reduced is at least  
657 transiently transformed to NO and possibly  $\text{N}_2$ . This transient pool of NO possibly stands in quasi-equilibrium with other  
658 intermediates (i.e.  $\text{HNO}$ ,  $\text{NO}_2(\text{g})$ ) or complexes (i.e. Fe-NO), and may thereby impact the overall reaction kinetics as well.  
659 We speculate that the transient accumulation of NO represents an important constraint both on overall reaction kinetics as well  
660 as on the  $\text{N}_2\text{O}$  isotopic signature (or  $\Delta^{15}\text{N}$ ), an aspect that should be verified in future work. Such work may include the  
661 quantification of  $\text{N}_2$  (and its N isotopic composition), which will help to assess to what extent (i) Fe-mineral surface-induced  
662 chemodenitrification leads to the formation of a transient pool of NO and is driven by the catalytically induced abiotic reaction  
663 between Fe(II) and  $\text{NO}_2^-$ , or if (ii) NO is actually the main oxidizing agent of Fe(II).  
664 Our data revealed further complexity with regards to N and O isotope effects during Fe-coupled chemodenitrification than  
665 previously reported. We argue that its isotopic imprint depends on the substrate concentration, the presence of reactive surfaces  
666 or other catalysts, the mechanisms induced by these catalysts (e.g. surface complexation), and putatively on the intermediates  
667 as well as on the product present at the end of the experiments. The multifaceted control on coupled N and O isotope

systematics in reactive N species may explain the discrepancies observed between our and previous work (e.g. with regards to  $^{15}\text{E}:$  $^{18}\text{E}$  ratios; Grabb et al. 2017). Clearly, one has to be realistic with regards to using  $\text{NO}_2^-$  and/or  $\text{N}_2\text{O}$  N and O isotope measurements to provide constraints on the relative importance of chemodenitrification under natural conditions. Yet, at this point, there is only a very limited number of studies on the isotope effects of chemodenitrification, and with the results presented here, we expand the body of work that aims at using stable isotope measurements to assess the occurrence of chemodenitrification in denitrifying environments. More work on the controls of stable isotope systematics of chemodenitrification, in particular on the role of reactive, and potentially cryptic, intermediate N species, and of O isotope exchange, will improve our ability to more quantitatively trace Fe-coupled nitrite reduction and  $\text{N}_2\text{O}$  production in natural Fe-rich soil or sedimentary environments.

**Data availability**

Data can be accessed upon request to the corresponding author.

**Author contributions**

AAK initiated the project. MFL and AAK supervised the project. ANV designed and conducted all experiments. Isotope measurements as well as data analysis were performed by ANV under the supervision of MFL. JMB conducted Mössbauer measurements and data analysis. PAN supervised and performed all  $\text{N}_2\text{O}$  concentration determination measurements. ANV, SDW and MFL interpreted the data and prepared the paper with inputs from all other co-authors.

**Competing interests**

The authors declare that they have no conflict of interest.

**Acknowledgements**

Special thanks go to Karen L. Casciotti (Stanford University) for helping with the correction of the  $\text{N}_2\text{O}$  isotope data. Thanks to Cindy-Louise Lockwood and Toby Samuels for corrections and comments on earlier versions of the manuscript, and to Viola Warter, Elizabeth Tomaszewski for fruitful discussions on abiotic chemistry and mineral reactions. Markus Maisch is thanked for his help with the preparation of the Mössbauer samples and Louis Rees for his help with cultivating *S. oneidensis* MR-1.

692 **Funding**

693 This research was supported by the Deutsche Forschungsgemeinschaft - DFG (Grants GRK 1708 Molecular principles of  
694 bacterial survival strategies), and through funds from the University of Basel, Switzerland.

695 **References**

- 696 Anderson, I. C. and Levine, J. S.: Relative Rates of Nitric Oxide and Nitrous Oxide Production by Nitrifiers, Denitrifiers, and  
697 Nitrate Respirers, *Appl. Environ. Microbiol.*, 51(5), 938–945, 1986.
- 698 Andrews, S. C., Robinson, A. K., Rodriguez-Quinones, F. and Rodríguez-Quinones, F.: Bacterial iron homeostasis, *FEMS*  
699 *Microbiol. Rev.*, 27(2–3), 215–237, doi:10.1016/s0168-6445(03)00055-x, 2003.
- 700 Baumgärtner, M. and Conrad, R.: Role of nitrate and nitrite for production and consumption of nitric oxide during  
701 denitrification in soil, *FEMS Microbiol. Lett.*, 101(1), 59–65, doi:10.1111/j.1574-6968.1992.tb05762.x, 1992.
- 702 Braun, V. and Hantke, K.: The Tricky Ways Bacteria Cope with Iron Limitation, pp. 31–66, Springer, Dordrecht., 2013.
- 703 Buchwald, C. and Casciotti, K. L.: Isotopic ratios of nitrite as tracers of the sources and age of oceanic nitrite, *Nat. Geosci.*,  
704 6(4), 308–313, doi:10.1038/ngeo1745, 2013.
- 705 Buchwald, C., Grabb, K., Hansel, C. M. and Wankel, S. D.: Constraining the role of iron in environmental nitrogen  
706 transformations: Dual stable isotope systematics of abiotic  $\text{NO}_2^-$  reduction by Fe(II) and its production of  $\text{N}_2\text{O}$ ,  
707 *Geochim. Cosmochim. Acta*, 186, 1–12, doi:http://dx.doi.org/10.1016/j.gca.2016.04.041, 2016.
- 708 Casciotti, K. L.: Inverse kinetic isotope fractionation during bacterial nitrite oxidation, *Geochim. Cosmochim. Acta*, 73(7),  
709 2061–2076, doi:10.1016/j.gca.2008.12.022, 2009.
- 710 Casciotti, K. L. and McIlvin, M. R.: Isotopic analyses of nitrate and nitrite from reference mixtures and application to Eastern  
711 Tropical North Pacific waters, *Mar. Chem.*, 107(2), 184–201, doi:10.1016/j.marchem.2007.06.021, 2007.
- 712 Casciotti, K. L., Boehlke, J. K., McIlvin, M. R., Mroczkowski, S. J., Hannon, J. E.: Oxygen isotopes in nitrite: Analysis,  
713 calibration, and equilibration, *Anal. Chem.*, 79(6), 2427–2436, doi:10.1021/ac061598h, 2007.
- 714 Chakraborty, A., Roden, E. E., Schieber, J. and Picardal, F.: Enhanced growth of *Acidovorax* sp. strain 2AN during nitrate-  
715 dependent Fe(II) oxidation in batch and continuous-flow systems., *Appl. Environ. Microbiol.*, 77(24), 8548–56,  
716 doi:10.1128/AEM.06214-11, 2011.
- 717 Charlet, L., Wersin, P. and Stumm, W.: Surface charge of  $\text{MnCO}_3$  and  $\text{FeCO}_3$ , *Geochim. Cosmochim. Acta*, 54(8), 2329–2336,  
718 doi:10.1016/0016-7037(90)90059-T, 1990.
- 719 Chen, D., Liu, T., Li, X., Li, F., Luo, X., Wu, Y. and Wang, Y.: Biological and chemical processes of microbially mediated  
720 nitrate-reducing Fe(II) oxidation by *Pseudogulbenkiania* sp. strain 2002, *Chem. Geol.*, 476, 59–69,  
721 doi:10.1016/j.chemgeo.2017.11.004, 2018.

722 Choi, P. S., Naal, Z., Moore, C., Casado-Rivera, E., Abruna, H. D., Helmann, J. D. and Shapleigh, J. P.: Assessing the Impact  
 723 of Denitrifier-Produced NO on other bacteria, Appl. Environ. Microbiol., 72(3), 2200–2205,  
 724 doi:10.1128/aem.72.3.2200-2205.2006, 2006.

725 Van Cleemput, O. and Samater, A.: Nitrite in soils: accumulation and role in the formation of gaseous N compounds, Fertil.  
 726 Res., 45(1), 81–89, doi:10.1007/BF00749884, 1995.

727 Coby, A. J. and Picardal, F. W.: Inhibition of NO<sub>3</sub><sup>-</sup> and NO<sub>2</sub><sup>-</sup> reduction by microbial Fe(III) reduction: Evidence of a reaction  
 728 between NO<sub>2</sub><sup>-</sup> and cell surface-bound Fe<sup>2+</sup>, Appl. Environ. Microbiol., 71(9), 5267–5274,  
 729 doi:10.1128/aem.71.9.5267-5274.2005, 2005.

730 Cornell, R. M. and Schwertmann, U.: The Iron Oxides: Structure, Properties, Reactions, Occurrences and Uses, 2nd ed., Wiley-  
 731 VCH., 2003.

732 Dai, Y.-F., Xiao, Y., Zhang, E.-H., Liu, L.-D., Qiu, L., You, L.-X., Dummi Mahadevan, G., Chen, B.-L. and Zhao, F.: Effective  
 733 methods for extracting extracellular polymeric substances from *Shewanella oneidensis* MR-1, Water Sci. Technol.,  
 734 74(12), 2987–2996, doi:10.2166/wst.2016.473, 2016.

735 Delahay, P., Pourbaix, M. and Rysselberghe, P. Van: Potential-pH diagrams, J. Chem. Educ. [online] Available from:  
 736 <https://pubs.acs.org/doi/pdfplus/10.1021/ed027p683> (Accessed 20 April 2018), 1950.

737 Dhakal, P.: Abiotic nitrate and nitrite reactivity with iron oxide minerals, University of Kentucky. [online] Available from:  
 738 [https://uknowledge.uky.edu/pss\\_etds/30](https://uknowledge.uky.edu/pss_etds/30), 2013.

739 Dhakal, P., Matocha, C. J., Huggins, F. E. and Vandiviere, M. M.: Nitrite Reactivity with Magnetite, Environ. Sci. Technol.,  
 740 47(12), 6206–6213, doi:10.1021/es304011w, 2013.

741 Doane, T. A.: The Abiotic Nitrogen Cycle, ACS Earth Sp. Chem., 1(7), 411–421, doi:10.1021/acsearthspacechem.7b00059,  
 742 2017.

743 Elsner, M.: Stable isotope fractionation to investigate natural transformation mechanisms of organic contaminants: principles,  
 744 prospects and limitations, J. Environ. Monit., 12(11), 2005–2031, doi:10.1039/c0em00277a, 2010.

745 Elsner, M., Schwarzenbach, R. P. and Haderlein, S. B.: Reactivity of Fe(II)-Bearing Minerals toward Reductive  
 746 Transformation of Organic Contaminants, Environ. Sci. Technol., 38(3), 799–807, doi:10.1021/es0345569, 2004.

747 Expert, D.: Iron, an Element Essential to Life, in Molecular Aspects of Iron Metabolism in Pathogenic and Symbiotic Plant-  
 748 Microbe Associations, pp. 1–6, Springer, Dordrecht., 2012.

749 Fowle, D. A. and Konhauser, K. O.: Microbial Surface Reactivity, pp. 614–616, Springer, Dordrecht., 2011.

750 Frame, C. H. and Casciotti, K. L.: Biogeochemical controls and isotopic signatures of nitrous oxide production by a marine  
 751 ammonia-oxidizing bacterium, Biogeosciences, 7(9), 2695–2709, doi:10.5194/bg-7-2695-2010, 2010.

752 Fry, B.: Stable Isotope Ecology, 3rd ed., Springer Science+Business Media, LLC, New York., 2006.

753 Goretski, J. and Hollocher, T. C.: Trapping of nitric oxide produced during denitrification by extracellular hemoglobin, J. Biol.  
 754 Chem., 263(5), 2316–2323 [online] Available from: <http://www.jbc.org/content/263/5/2316.abstract>, 1988.

755 Gorski, C. A. and Scherer, M. M.: Fe<sup>2+</sup> sorption at the Fe oxide-water interface: A revised conceptual framework, in Aquatic  
 756 Redox Chemistry, vol. 1071, edited by P. G. Tratnyek, T. J. Grundl, and S. B. Haderlein, pp. 315–343, ACS  
 757 Publications., 2011.

758 Grabb, K. C., Buchwald, C., Hansel, C. M. and Wankel, S. D.: A dual nitrite isotopic investigation of chemodenitrification by  
 759 mineral-associated Fe(II) and its production of nitrous oxide, *Geochim. Cosmochim. Acta*, 196, 388–402 [online]  
 760 Available from: <https://www.sciencedirect.com/science/article/pii/S0016703716306044> (Accessed 28 March 2019),  
 761 2017.

762 Granger, J. and Sigman, D. M.: Removal of nitrite with sulfamic acid for nitrate N and O isotope analysis with the denitrifier  
 763 method, *Rapid Commun. Mass Spectrom.*, 23(23), 3753–3762, doi:10.1002/rcm.4307, 2009.

764 Granger, J., Sigman, D. M., Lehmann, M. F. and Tortell, P. D.: Nitrogen and oxygen isotope fractionation during dissimilatory  
 765 nitrate reduction by denitrifying bacteria, *Limnol. Oceanogr.*, 53(6), 2533–2545, doi:10.4319/lo.2008.53.6.2533,  
 766 2008.

767 Granger, J., Karsh, K. L., Guo, W., Sigman, D. M. and Kritee, K.: The nitrogen and oxygen isotope composition of nitrate in  
 768 the environment: The systematics of biological nitrate reduction, *Geochim. Cosmochim. Acta*, 73(13), A460–A460,  
 769 2009.

770 Halder, S., Yadav, K. K., Sarkar, R., Mukherjee, S., Saha, P., Haldar, S., Karmakar, S. and Sen, T.: Alteration of Zeta potential  
 771 and membrane permeability in bacteria: a study with cationic agents., *Springerplus*, 4, 672, doi:10.1186/s40064-015-  
 772 1476-7, 2015.

773 He, H., Zhang, S., Zhu, C. and Liu, Y.: Equilibrium and kinetic Si isotope fractionation factors and their implications for Si  
 774 isotope distributions in the Earth's surface environments, *Acta Geochim.*, 35(1), 15–24, doi:10.1007/s11631-015-  
 775 0079-x, 2016a.

776 He, S., Tominski, C., Kappler, A. A., Behrens, S. and Roden, E. E.: Metagenomic analyses of the autotrophic Fe(II)-oxidizing,  
 777 nitrate-reducing enrichment culture KS, *Appl. Environ. Microbiol.*, 82(9), 2656–2668, doi:10.1128/AEM.03493-15,  
 778 2016b.

779 Heidelberg, J. F., Paulsen, I. T., Nelson, K. E., Gaidos, E. J., Nelson, W. C., Read, T. D., Eisen, J. A., Seshadri, R., Ward, N.,  
 780 Methe, B., Clayton, R. A., Meyer, T., Tsapin, A., Scott, J., Beanan, M., Brinkac, L., Daugherty, S., DeBoy, R. T.,  
 781 Dodson, R. J., Durkin, A. S., Haft, D. H., Kolonay, J. F., Madupu, R., Peterson, J. D., Umayam, L. A., White, O.,  
 782 Wolf, A. M., Vamathevan, J., Weidman, J., Impraim, M., Lee, K., Berry, K., Lee, C., Mueller, J., Khouri, H., Gill, J.,  
 783 Utterback, T. R., McDonald, L. A., Feldblyum, T. V., Smith, H. O., Venter, J. C., Neelson, K. H. and Fraser, C. M.:  
 784 Genome sequence of the dissimilatory metal ion-reducing bacterium *Shewanella oneidensis*, *Nat. Biotechnol.*,  
 785 20(11), 1118–1123, doi:10.1038/nbt749, 2002.

786 Heil, J., Vereecken, H. and Brüggemann, N.: A review of chemical reactions of nitrification intermediates and their role in  
 787 nitrogen cycling and nitrogen trace gas formation in soil, *Eur. J. Soil Sci.*, 67(1), 23–39, doi:10.1111/ejss.12306,  
 788 2016.

789 Hunkeler, D. and Elsner, M.: Principles and Mechanisms of Isotope Fractionation, in Environmental Isotopes in  
 790 Biodegradation and Bioremediation, edited by Aelion, C.M., Höhener, P., Hunkeler, D., and Aravena, R., pp. 43–76,  
 791 CRC Press., 2009.

792 Ilbert, M. and Bonnefoy, V.: Insight into the evolution of the iron oxidation pathways, *Biochim. Biophys. Acta - Bioenerg.*,  
 793 1827(2), 161–175, doi:http://dx.doi.org/10.1016/j.bbabo.2012.10.001, 2013.

794 Jamieson, J., Prommer, H., Kaksonen, A. H., Sun, J., Siade, A. J., Yusov, A. and Bostick, B.: Identifying and Quantifying the  
 795 Intermediate Processes during Nitrate-Dependent Iron(II) Oxidation, *Environ. Sci. Technol.*, acs.est.8b01122,  
 796 doi:10.1021/acs.est.8b01122, 2018.

797 Jones, L. C., Peters, B., Lezama Pacheco, J. S., Casciotti, K. L. and Fendorf, S.: Stable Isotopes and Iron Oxide Mineral  
 798 Products as Markers of Chemodenitrification, *Environ. Sci. Technol.*, 49(6), 3444–3452, doi:10.1021/es504862x,  
 799 2015.

800 Kampschreur, M. J., Kleerebezem, R., de Vet, W. and van Loosdrecht, M.: Reduced iron induced nitric oxide and nitrous  
 801 oxide emission, *Water Res.*, 45(18), 5945–5952, doi:http://dx.doi.org/10.1016/j.watres.2011.08.056, 2011.

802 Kendall, C. and Aravena, R.: Nitrate Isotopes in Groundwater Systems, *Environmental Tracers in Subsurface Hydrology*, 261–  
 803 297, doi:10.1007/978-1-4615-4557-6\_9, 2000.

804 Klueglein, N. and Kappler, A. A.: Abiotic oxidation of Fe(II) by reactive nitrogen species in cultures of the nitrate-reducing  
 805 Fe(II) oxidizer *Acidovorax* sp BoFeN1 - questioning the existence of enzymatic Fe(II) oxidation, *Geobiology*, 11(2),  
 806 396, doi:10.1111/gbi.12040, 2013.

807 Klueglein, N., Zeitvogel, F., Stierhof, Y.-D., Floetenmeyer, M., Konhauser, K. O., Kappler, A. A. and Obst, M.: Potential Role  
 808 of Nitrite for Abiotic Fe(II) Oxidation and Cell Encrustation during Nitrate Reduction by Denitrifying Bacteria, *Appl.*  
 809 *Environ. Microbiol.*, 80(3), 1051–1061, doi:10.1128/aem.03277-13, 2014.

810 Lagarec, K. and Rancourt, D. G.: Extended Voigt-based analytic lineshape method for determining N-dimensional correlated  
 811 hyperfine parameter distributions in Mössbauer spectroscopy, *Nucl. Instruments Methods Phys. Res. Sect. B Beam*  
 812 *Interact. with Mater. Atoms*, 129(2), 266–280, doi:10.1016/S0168-583X(97)00284-X, 1997.

813 Laufer, K., Røy, H., Jørgensen, B. B. and Kappler, A. A.: Evidence for the existence of autotrophic nitrate-reducing Fe(II)-  
 814 oxidizing bacteria in marine coastal sediment, *Appl. Environ. Microbiol.*, 82(20), 6120–6131,  
 815 doi:10.1128/AEM.01570-16, 2016.

816 Li, W., Beard, B. L. and Johnson, C. M.: Exchange and fractionation of Mg isotopes between epsomite and saturated MgSO<sub>4</sub>  
 817 solution, *Geochim. Cosmochim. Acta*, 75, 1814–1828, doi:10.1016/j.gca.2011.01.023, 2011.

818 Lies, D. P., Hernandez, M. E., Kappler, A. A., Mielke, R. E., Gralnick, J. A. and Newman, D. K.: *Shewanella oneidensis* MR-  
 819 1 uses overlapping pathways for iron reduction at a distance and by direct contact under conditions relevant for  
 820 biofilms, *Appl. Environ. Microbiol.*, 71(8), 4414–4426, doi:10.1128/aem.71.8.4414-4426.2005, 2005.

821 Liu, J. and Konermann, L.: Irreversible Thermal Denaturation of cytochrome-c studied by Electrospray Mass Spectrometry, *J.*  
 822 *Am. Soc. Mass Spectrom.*, 20(5), 819–828, doi:10.1016/J.JASMS.2008.12.016, 2009.

823 Liu, J., Wang, Z., Belchik, S. M., Edwards, M. J., Liu, C., Kennedy, D. W., Merkley, E. D., Lipton, M. S., Butt, J. N.,  
 824 Richardson, D. J., Zachara, J. M., Fredrickson, J. K., Rosso, K. M. and Shi, L.: Identification and Characterization of  
 825 MtoA: A Decaheme c-Type Cytochrome of the Neutrophilic Fe(II)-Oxidizing Bacterium *Sideroxydans lithotrophicus*  
 826 ES-1., *Front. Microbiol.*, 3, 37, doi:10.3389/fmicb.2012.00037, 2012.

827 Liu, T., Chen, D., Luo, X., Li, X. and Li, F.: Microbially mediated nitrate-reducing Fe(II) oxidation: Quantification of  
 828 chemodenitrification and biological reactions, *Geochim. Cosmochim. Acta*, doi:10.1016/J.GCA.2018.06.040, 2018.

829 Lovley, D. R.: Microbial Fe(III) reduction in subsurface environments, *FEMS Microbiol. Rev.*, 20(3–4), 305–313,  
 830 doi:10.1111/j.1574-6976.1997.tb00316.x, 1997.

831 Lovley, D. R.: Electromicrobiology, *Annu. Rev. Microbiol.*, 66(1), 391–409, doi:10.1146/annurev-micro-092611-150104,  
 832 2012.

833 Luan, F., Liu, Y., Griffin, A. M., Gorski, C. A. and Burgos, W. D.: Iron(III)-Bearing Clay Minerals Enhance Bioreduction of  
 834 Nitrobenzene by *Shewanella putrefaciens* CN32, *Env. Sci Technol*, 49, 1418–1476, doi:10.1021/es504149y, 2015.

835 Luna-Zaragoza, D., Romero-Guzmán, E. T. and Reyes-Gutiérrez, L. R.: Surface and Physicochemical Characterization of  
 836 Phosphates Vivianite and Hydroxyapatite, *J. Miner. Mater. Charact. Eng.*, 08(08), 591–609,  
 837 doi:10.4236/jmmce.2009.88052, 2009.

838 Mariotti, A., Germon, J. C., Hubert, P., Kaiser, P., Letolle, R., Tardieux, A. and Tardieux, P.: Experimental determination of  
 839 nitrogen kinetic isotope fractionation: Some principles; illustration for the denitrification and nitrification processes,  
 840 *Plant Soil*, 62(3), 413–430, doi:10.1007/BF02374138, 1981.

841 Martin, T. S. and Casciotti, K. L.: Paired N and O isotopic analysis of nitrate and nitrite in the Arabian Sea oxygen deficient  
 842 zone, *Deep. Res. Part I Oceanogr. Res. Pap.*, 121, 121–131, doi:10.1016/j.dsr.2017.01.002, 2017.

843 McIlvin, M. R. and Altabet, M. A.: Chemical conversion of nitrate and nitrite to nitrous oxide for nitrogen and oxygen isotopic  
 844 analysis in freshwater and seawater, *Anal. Chem.*, 77(17), 5589–5595, doi:10.1021/ac050528s, 2005.

845 McIlvin, M. R. and Casciotti, K. L.: Fully automated system for stable isotopic analyses of dissolved nitrous oxide at natural  
 846 abundance levels, *Limnol. Oceanogr. Methods*, 8(2), 54–66, doi:10.4319/lom.2010.8.54, 2010.

847 McKnight, G. M., Smith, L. M., Drummond, R. S., Duncan, C. W., Golden, M. and Benjamin, N.: Chemical synthesis of nitric  
 848 oxide in the stomach from dietary nitrate in humans., *Gut*, 40(2), 211–4 [online] Available from:  
 849 <http://www.ncbi.nlm.nih.gov/pubmed/9071933> (Accessed 18 March 2018), 1997.

850 Minguzzi, A., Fan, F.-R. F., Vertova, A., Rondinini, S. and Bard, A. J.: Dynamic potential–pH diagrams application to  
 851 electrocatalysts for wateroxidation, *Chem. Sci.*, 3(1), 217–229, doi:10.1039/C1SC00516B, 2012.

852 Mohn, J., Wolf, B., Toyoda, S., Lin, C.-T., Liang, M.-C., Brüggemann, N., Wissel, H., Steiker, A. E., Dyckmans, J., Szewc,  
 853 L., Ostrom, N. E., Casciotti, K. L., Forbes, M., Giesemann, A., Well, R., Doucett, R. R., Yarnes, C. T., Ridley, A. R.,  
 854 Kaiser, J. and Yoshida, N.: Interlaboratory assessment of nitrous oxide isotopomer analysis by isotope ratio mass  
 855 spectrometry and laser spectroscopy: current status and perspectives, *Rapid Commun. Mass Spectrom.*, 28(18), 1995–  
 856 2007, doi:10.1002/rcm.6982, 2014.



857 Muehe, E. M., Gerhardt, S., Schink, B. and Kappler, A.: Ecophysiology and the energetic benefit of mixotrophic Fe(II)  
 858 oxidation by various strains of nitrate-reducing bacteria, *FEMS Microbiol. Ecol.*, 70(3), 335–343, doi:10.1111/j.1574-  
 859 6941.2009.00755.x, 2009.

860 Muehe, E. M., Obst, M., Hitchcock, A., Tyliczszak, T., Behrens, S., Schröder, C., Byrne, J. M., Michel, F. M., Krämer, U. and  
 861 Kappler, A. A.: Fate of Cd during microbial Fe(III) mineral reduction by a novel and Cd-tolerant geobacter species,  
 862 *Environ. Sci. Technol.*, 47(24), 14099–14109, doi:10.1021/es403365w, 2013.

863 Nelson, D. W. and Bremner, J. M.: Factors affecting chemical transformations of nitrite in soils, *Soil Biol. Biochem.*, 1(3),  
 864 229–239, doi:10.1016/0038-0717(69)90023-6, 1969.

865 Niklaus, P. A., Le Roux, X., Poly, F., Buchmann, N., Scherer-Lorenzen, M., Weigelt, A. and Barnard, R. L.: Plant species  
 866 diversity affects soil–atmosphere fluxes of methane and nitrous oxide, *Oecologia*, 181(3), 919–930,  
 867 doi:10.1007/s00442-016-3611-8, 2016.

868 Nordhoff, M., Tominski, C., Halama, M., Byrne, J. M., Obst, M., Kleindienst, S., Behrens, S. and Kappler, A. A.: Insights into  
 869 nitrate-reducing Fe(II) oxidation mechanisms through analysis of cell-mineral associations, cell encrustation, and  
 870 mineralogy in the chemolithoautotrophic enrichment culture KS, *Appl. Environ. Microbiol.*, 83(13), e00752-17,  
 871 doi:10.1128/AEM.00752-17, 2017.

872 Ostrom, N. E. and Ostrom, P.: *Handbook of Environmental Isotope Geochemistry*, 1st ed., edited by M. Baskaran, Springer  
 873 Berlin Heidelberg, Berlin, Heidelberg., 2011.

874 Ostrom, N. E. and Ostrom, P. H.: The Isotopomers of Nitrous Oxide: Analytical Considerations and Application to Resolution  
 875 of Microbial Production Pathways, in *Handbook of Environmental Isotope Geochemistry: Vol I*, edited by M.  
 876 Baskaran, pp. 453–476, Springer Berlin Heidelberg, Berlin, Heidelberg., 2012.

877 Ostrom, N. E., Pitt, A., Sutka, R., Ostrom, P. H., Grandy, A. S., Huizinga, K. M. and Robertson, G. P.: Isotopologue effects  
 878 during N<sub>2</sub>O reduction in soils and in pure cultures of denitrifiers, *J. Geophys. Res.*, 112(G2),  
 879 doi:10.1029/2006jg000287, 2007.

880 Ostrom, N. E., Gandhi, H., Coplen, T. B., Toyoda, S., Böhlke, J. K., Brand, W. A., Casciotti, K. L., Dyckmans, J., Giesemann,  
 881 A., Mohn, J., Well, R., Yu, L. and Yoshida, N.: Preliminary assessment of stable nitrogen and oxygen isotopic  
 882 composition of USGS51 and USGS52 nitrous oxide reference gases and perspectives on calibration needs, *Rapid*  
 883 *Commun. Mass Spectrom.*, 32(15), 1207–1214, doi:10.1002/rcm.8157, 2018.

884 Otte, J. M., Blackwell, N., Ruser, R., Kappler, A. A., Kleindienst, S. and Schmidt, C.: N<sub>2</sub>O formation by nitrite-induced  
 885 (chemo)denitrification in coastal marine sediment, *Sci. Rep.*, 9(1), 10691, doi:10.1038/s41598-019-47172-x, 2019.

886 Ottley, C. J., Davison, W. and Edmunds, W. M.: Chemical catalysis of nitrate reduction by iron(II), *Geochim. Cosmochim.*  
 887 *Acta*, 61(9), 1819–1828, doi:10.1016/S0016-7037(97)00058-6, 1997.

888 Pereira, C., Ferreira, N. R., Rocha, B. S., Barbosa, R. M. and Laranjinha, J.: The redox interplay between nitrite and nitric  
 889 oxide: From the gut to the brain, *Redox Biol.*, 1(1), 276–284, doi:http://dx.doi.org/10.1016/j.redox.2013.04.004,  
 890 2013.

891 Phillips, R. L., Song, B., McMillan, A. M. S., Grelet, G., Weir, B. S., Palmada, T. and Tobias, C.: Chemical formation of  
 892 hybrid di-nitrogen calls fungal codenitrification into question, *Sci. Rep.*, 6(1), 39077, doi:10.1038/srep39077, 2016.

893 Piasecki, W., Szymanek, K. and Charmas, R.: Fe<sup>2+</sup> adsorption on iron oxide: the importance of the redox potential of the  
 894 adsorption system, *Adsorption*, doi:10.1007/s10450-019-00054-0, 2019.

895 Piepenbrock, A., Dippon, U., Porsch, K., Appel, E. and Kappler, A. A.: Dependence of microbial magnetite formation on  
 896 humic substance and ferrihydrite concentrations, *Geochim. Cosmochim. Acta*, 75(22), 6844–6858,  
 897 doi:10.1016/j.gca.2011.09.007, 2011.

898 Price, A., Macey, M. C., Miot, J. and Olsson-Francis, K.: Draft Genome Sequences of the Nitrate-Dependent Iron-Oxidizing  
 899 Proteobacteria *Acidovorax* sp. Strain BoFeN1 and *Paracoccus pantotrophus* Strain KS1, edited by J. C. Thrash,  
 900 *Microbiol. Resour. Announc.*, 7(10), e01050-18, doi:10.1128/mra.01050-18, 2018.

901 Rakshit, S., Matocha, C. J. and Coyne, M. S.: Nitrite reduction by siderite, *Soil Sci. Soc. Am. J.*, 72(4), 1070–1077,  
 902 doi:10.2136/sssaj2007.0296, 2008.

903 Rancourt, D. G. and Ping, J. Y.: Voigt-based methods for arbitrary-shape static hyperfine parameter distributions in Mössbauer  
 904 spectroscopy, *Nucl. Instruments Methods Phys. Res. Sect. B Beam Interact. with Mater. Atoms*, 58(1), 85–97,  
 905 doi:10.1016/0168-583X(91)95681-3, 1991.

906 Rivallan, M., Ricchiardi, G., Bordiga, S. and Zecchina, A.: Adsorption and reactivity of nitrogen oxides (NO<sub>2</sub>, NO, N<sub>2</sub>O) on  
 907 Fe-zeolites, *J. Catal.*, 264(2), 104–116, doi:10.1016/j.jcat.2009.03.012, 2009.

908 Samarkin, V. A., Madigan, M. T., Bowles, M. W., Casciotti, K. L., Priscu, J. C., McKay, C. P. and Joye, S. B.: Abiotic nitrous  
 909 oxide emission from the hypersaline Don Juan Pond in Antarctica, *Nat. Geosci.*, 3(5), 341–344, doi:10.1038/ngeo847,  
 910 2010.

911 Schaefer, M. V.: Spectroscopic evidence for interfacial Fe(II)- Fe(III) electron transfer in clay minerals, Iowa Research Online.  
 912 [online] Available from: <http://ir.uiowa.edu/etd/596> (Accessed 20 March 2018), 2010.

913 Sigman, D. M., DiFiore, P. J., Hain, M. P., Deutsch, C., Wang, Y., Karl, D. M., Knapp, A. N., Lehmann, M. F. and Pantoja,  
 914 S.: The dual isotopes of deep nitrate as a constraint on the cycle and budget of oceanic fixed nitrogen, *Deep. Res. Part*  
 915 *I-Oceanographic Res. Pap.*, 56(9), 1419–1439, doi:10.1016/j.dsr.2009.04.007, 2009.

916 Snyder, L. R. and Adler, H. J.: Dispersion in Segmented Flow through Glass Tubing in Continuous-Flow Analysis: The Ideal  
 917 Model, *Anal. Chem.*, 48(7), 1017–1022, doi:10.1021/ac60371a013, 1976.

918 Sorensen, J. and Thorling, L.: Stimulation by Lepidocrocite (Gamma-FeOOH) of Fe(II)-Dependent Nitrite Reduction, *Geochim.*  
 919 *Cosmochim. Acta*, 55(5), 1289–1294, doi:10.1016/0016-7037(91)90307-Q, 1991.

920 Stevenson, F. J., Harrison, R. M., Wetselaar, R. and Leeper, R. A.: Nitrosation of Soil Organic Matter: III. Nature of Gases  
 921 Produced by Reaction of Nitrite with Lignins, Humic Substances, and Phenolic Constituents Under Neutral and  
 922 Slightly Acidic Conditions1, *Soil Sci. Soc. Am. J.*, 34(3), 430, doi:10.2136/sssaj1970.03615995003400030024x,  
 923 1970.

924 Stookey, L. L.: Ferrozine - A new spectrophotometric reagent for iron, *Anal. Chem.*, 42(7), 779-, doi:10.1021/ac60289a016,  
 925 1970.

926 Straub, K. L., Benz, M., Schink, B. and Widdel, F.: Anaerobic, nitrate-dependent microbial oxidation of ferrous iron, *Appl.*  
 927 *Environ. Microbiol.*, 62(4), 1458–1460, 1996.

928 Stumm, W. and Sulzberger, B.: The cycling of iron in natural environments: Considerations based on laboratory studies of  
 929 heterogeneous redox processes, *Geochim. Cosmochim. Acta*, 56(8), 3233–3257, doi:10.1016/0016-7037(92)90301-  
 930 X, 1992.

931 Sutka, R. L., Ostrom, N. E., Ostrom, P. H., Breznak, J. A., Gandhi, H., Pitt, A. J. and Li, F.: Distinguishing nitrous oxide  
 932 production from nitrification and denitrification on the basis of isotopomer abundances, *Appl. Environ. Microbiol.*,  
 933 72(1), 638–644, doi:10.1128/Aem.72.1.638-644.2006, 2006.

934 Tanford, C.: Protein denaturation: Part c. theoretical models for the mechanism of denaturation, *Adv. Protein Chem.*, 24(C),  
 935 1–95, doi:10.1016/S0065-3233(08)60241-7, 1970.

936 Taran, Y. A., Kliger, G. A., Cienfuegos, E. and Shuykin, A. N.: Carbon and hydrogen isotopic compositions of products of  
 937 open-system catalytic hydrogenation of CO<sub>2</sub>: Implications for abiogenic hydrocarbons in Earth's crust, *Geochim.*  
 938 *Cosmochim. Acta*, 74(21), 6112–6125, doi:10.1016/j.gca.2010.08.012, 2010.

939 Tian, T., Zhou, K., Xuan, L., Zhang, J.-X., Li, Y.-S., Liu, D.-F. and Yu, H.-Q.: Exclusive microbially driven autotrophic iron-  
 940 dependent denitrification in a reactor inoculated with activated sludge, *Water Res.*, 170, 115300,  
 941 doi:10.1016/j.watres.2019.115300, 2020.

942 Tiso, M. and Schechter, A. N.: Nitrate reduction to nitrite, nitric oxide and ammonia by gut bacteria under physiological  
 943 conditions., *PLoS One*, 10(3), e0119712, doi:10.1371/journal.pone.0119712, 2015.

944 Tominski, C., Heyer, H., Lösekann-Behrens, T., Behrens, S. and Kappler, A. A.: Growth and Population Dynamics of the  
 945 Anaerobic Fe(II)-Oxidizing and Nitrate-Reducing Enrichment Culture KS, edited by F. E. Löffler, *Appl. Environ.*  
 946 *Microbiol.*, 84(9), e02173-17, doi:10.1128/AEM.02173-17, 2018.

947 Toyoda, S. and Yoshida, N.: Determination of Nitrogen Isotopomers of Nitrous Oxide on a Modified Isotope Ratio Mass  
 948 Spectrometer, , doi:10.1021/AC9904563, 1999.

949 Toyoda, S., Mutoke, H., Yamagishi, H., Yoshida, N. and Tanji, Y.: Fractionation of N<sub>2</sub>O isotopomers during production by  
 950 denitrifier, *Soil Biol. Biochem.*, 37(8), 1535–1545, doi:10.1016/j.soilbio.2005.01.009, 2005.

951 Veeramani, H., Alessi, D. S., Suvorova, E. I., Lezama-Pacheco, J. S., Stubbs, J. E., Sharp, J. O., Dippon, U., Kappler, A. A.,  
 952 Bargar, J. R. and Bernier-Latmani, R.: Products of abiotic U(VI) reduction by biogenic magnetite and vivianite,  
 953 *Geochim. Cosmochim. Acta*, 75(9), 2512–2528, doi:10.1016/j.gca.2011.02.024, 2011.

954 Wankel, S. D., Ziebis, W., Buchwald, C., Charoenpong, C., De Beer, Di., Dentinger, J., Xu, Z. and Zengler, K.: Evidence for  
 955 fungal and chemodenitrification based N<sub>2</sub>O flux from nitrogen impacted coastal sediments, *Nat. Commun.*, 8(1),  
 956 15595, doi:10.1038/ncomms15595, 2017.

957 Weber, K. A., Hedrick, D. B., Peacock, A. D., Thrash, J. C., White, D. C., Achenbach, L. A. and Coates, J. D.: Physiological  
 958 and taxonomic description of the novel autotrophic, metal oxidizing bacterium, *Pseudogulbenkiania* sp. strain 2002,  
 959 Appl. Microbiol. Biotechnol., 83(3), 555–565, doi:10.1007/s00253-009-1934-7, 2009.

960 Well, R. and Flessa, H.: Isotopologue signatures of N<sub>2</sub>O produced by denitrification in soils, J. Geophys. Res., 114,  
 961 doi:10.1029/2008jg000804, 2009.

962 Wenk, C. B., Frame, C. H., Koba, K., Casciotti, K. L., Veronesi, M., Niemann, H., Schubert, C. J., Yoshida, N., Toyoda, S.,  
 963 Makabe, A., Zopfi, J. and Lehmann, M. F.: Differential N<sub>2</sub>O dynamics in two oxygen-deficient lake basins revealed  
 964 by stable isotope and isotopomer distributions, Limnol. Oceanogr., 61(5), 1735–1749, doi:10.1002/lno.10329, 2016.

965 White, G. F., Edwards, M. J., Gomez-Perez, L., Richardson, D. J., Butt, J. N. and Clarke, T. A.: Mechanisms of Bacterial  
 966 Extracellular Electron Exchange, in Advances in Microbial Physiology, vol. 68, pp. 87–138., 2016.

967 Widdel, F. and Pfennig, N.: Studies on dissimilatory Sulfate-reducing Bacteria that decompose Fatty-Acids - 1. Isolation of  
 968 New Sulfate-reducing Bacteria enriched with Acetate from saline Environments - Description of Desulfobacter  
 969 postgatei gen. nov. sp. nov., Arch. Microbiol., 129(5), 395–400, doi:10.1007/bf00406470, 1981.

970 Widdel, F., Kohring, G.-W. and Mayer, F.: Studies on Dissimilatory Sulfate-Reducing Bacteria that Decompose Fatty Acids,  
 971 Arch Microbiol, 134, 286–294 [online] Available from:  
 972 <https://link.springer.com/content/pdf/10.1007/BF00407804.pdf> (Accessed 22 April 2018), 1983.

973 Wilson, W. W., Wade, M. M., Holman, S. C. and Champlin, F. R.: Status of methods for assessing bacterial cell surface charge  
 974 properties based on zeta potential measurements, J. Microbiol. Methods, 43(3), 153–164, doi:10.1016/S0167-  
 975 7012(00)00224-4, 2001.

976 Winther, M., Balslev-Harder, D., Christensen, S., Priemé, A., Elberling, B., Crosson, E. and Blunier, T.: Continuous  
 977 measurements of nitrous oxide isotopomers during incubation experiments, Biogeosciences, 15(3), 767–780,  
 978 doi:10.5194/bg-15-767-2018, 2018.

979 Wunderlin, P., Lehmann, M. F., Siegrist, H., Tuzson, B., Joss, A., Emmenegger, L. and Mohn, J.: Isotope Signatures of N<sub>2</sub>O  
 980 in a Mixed Microbial Population System: Constraints on N<sub>2</sub>O Producing Pathways in Wastewater Treatment, Environ.  
 981 Sci. Technol., 130118101927005, doi:10.1021/es303174x, 2013.

982 Ye, R. W., Averill, B. A. and Tiedje, J. M.: Denitrification: production and consumption of nitric oxide, Appl. Environ.  
 983 Microbiol., 60(4), 1053–1058 [online] Available from: <http://www.ncbi.nlm.nih.gov/pmc/articles/PMC201439/>,  
 984 1994.

985 Zeitvogel, F., Burkhardt, C. J., Schroepel, B., Schmid, G., Ingino, P. and Obst, M.: Comparison of Preparation Methods of  
 986 Bacterial Cell-Mineral Aggregates for SEM Imaging and Analysis Using the Model System of *Acidovorax* sp.  
 987 BoFeN1, Geomicrobiol. J., 34(4), 317–327, doi:10.1080/01490451.2016.1189467, 2017.

988 Zhu-Barker, X., Cavazos, A. R., Ostrom, N. E., Horwath, W. R. and Glass, J. B.: The importance of abiotic reactions for  
 989 nitrous oxide production, Biogeochemistry, 126(3), 251–267, doi:10.1007/s10533-015-0166-4, 2015.

990 Zumft, W. G.: Cell biology and molecular basis of denitrification, *Microbiol. Mol. Biol. Rev.*, 61(4), [online] Available from:  
991 <http://www.ncbi.nlm.nih.gov/pubmed/9409151> (Accessed 19 February 2018), 1997.  
992 Zweier, J. L., Samouilov, A. and Kuppasamy, P.: Non-enzymatic nitric oxide synthesis in biological systems, *Biochim.*  
993 *Biophys. Acta - Bioenerg.*, 1411(2–3), 250–262, doi:10.1016/S0005-2728(99)00018-3, 1999.  
994